

Journal of Materials Science

Volume No. 11

Issue No. 3

September - December 2023



ENRICHED PUBLICATIONS PVT. LTD

**S-9, IInd FLOOR, MLU POCKET,
MANISH ABHINAV PLAZA-II, ABOVE FEDERAL BANK,
PLOT NO-5, SECTOR-5, DWARKA, NEW DELHI, INDIA-110075,
PHONE: - + (91)-(11)-47026006**

Journal of Materials Science

Aims and Scope

The Journal of Materials Science is now firmly established as the leading source of primary communication for scientists investigating the structure and properties of all engineering materials. The Journal of Materials Science publishes reviews, full-length papers, and short communications recording original research results on, or techniques for studying the relationship between structure, properties, and uses of materials. The subjects are seen from international and interdisciplinary perspectives covering areas including metals, ceramics, glasses, polymers, electrical materials, composite materials, fibers, nanostructured materials, nanocomposites, and biological and biomedical materials.

Journal of Materials Science

Managing Editor
Mr. Amit Prasad

Editor in Chief

Dr. Devinder Singh
DST Inspire Faculty
Department of Physics
Punjab University, Chandigarh 160014
devinderpu@pu.ac.in

Dr. Gurbhinder Singh Brar
Guru Kashi University,
Talwandi Sabo
gurbhindersinghbrar@gmail.com

Journal of Materials Science

(Volume No. 11, Issue No. 3, September - December 2023)

Contents

Sr. No.	Articles / Authors Name	Pg. No.
1	Parametric Optimization of Mig Process Parameters using Taguchi and Grey Taguchi Analysis – <i>Dinesh Mohan Arya, Vedansh Chaturvedi, Jyoti Vimal</i>	101 - 112
2	Principal Stress Analysis of Luffing Jib Using Solid Works - 12 – <i>Atul shanker suman, Jyoti vimal, Vedansh chaturvedi</i>	113 - 120
3	Wear Rate of (Aluminium) AL-6061 on Different Loads – <i>Rahul Jaiswal</i>	121 - 126
4	MHD Flow and Heat Transfer of A Non-Newtonian Law Fluid Past A Stretching Sheet with Heat Generation/absorption – <i>B. Shashidar Reddy</i>	127 - 136
5	Measurement of Radiation from Naturally Occurring Radioactive Materials in a Mineral Called “Ewoa”, Gurage zone, Ethiopia. – <i>T. Tessema Teklemariam, W. Tsegaye Birhanu</i>	137 - 144
6	Heat Generation and Uniform Suction/Blowing of Micropolar Fluid Flow on Porous Plat with Temperature Dependent Viscosity and Thermal Conductivity – <i>Bhairab Borgohian</i>	145 - 151

Parametric Optimization of Mig Process Parameters using Taguchi and Grey Taguchi Analysis

Dinesh Mohan Arya* Vedansh Chaturvedi Jyoti Vimal****

*Research Scholar, Department of Mechanical Engineering, Madhav Institute of Technology & Science, Gwalior

**Assistant Professor, Department of Mechanical Engineering, Madhav Institute of Technology & Science, Gwalior

ABSTRACT

The aim of this study is to investigate the optimization process parameters for Metal inert gas welding (MIG). The optimization of MIG welding operating parameters are for alloy steel work piece using grey relational analysis method. Sixteen experimental runs based on an orthogonal array Taguchi method were performed. This paper presents the influence of welding parameters like wire diameter, welding current, arc voltage, welding speed, and gas flow rate optimization based on bead geometry of welding joint. The objective function have been chosen in relation to parameters of MIG welding bead geometry Tensile strength, Bead width, Bead height, Penetration and Heat affected zone (HAZ) for quality target. Optimal parameters contribution of the MIG operation was obtained via grey relational analysis. By analysis the grey relational grade, preprocessed data, and grey relational coefficient of grey relational controllable process factor on the individual quality characteristic targets additionally the analysis of variance (ANOVA) is also applied to identify the welding current is the most significant factor. Experiment with the optimized parameter setting, which have been obtained from the analysis, are giving to validate the results.

Keywords:-MIG Welding, Grey relational analysis, Taguchi orthogonal array, Analysis of variance(ANOVA).

1. INTRODUCTION

MIG (Metal Inert Gas) welding, also known as MAG (Metal Active Gas) and in the USA as GMAW (Gas Metal Arc Welding), is a welding process that is now widely used for welding a variety of materials, ferrous and non ferrous.[1]

In gas shielded arc welding both the arc and the molten weld pool are shielded from the atmosphere by a stream of gas. The arc may be produced between a continuously fed wire and the work. The shielding gas can be both inert gas like argon and active gases like argon-oxygen mixture and carbon-di-oxide which are chemically reactive. It can be used on nearly all metals including carbon steel, stainless steel, alloy steel and aluminum. Arc travel speed is typically 30- 38 cm/minute and weld metal deposition rate varies from 1.25 kg/hr when welding out of position to 5.5 kg/hr in flat position.[8]

Metal transfer across the arc, is short circuiting transfer, globular transfer, spray transfer, pulsed spray transfer. The made of weld metal transfer is determined by the following welding current, electrode size, electrode composition, electrode stick out, shielding gas. Joint type in MIG welding, the most commonly used joint type are the butt joint, corner joint, edge joint, lap joint and T-joint.[1] A metal inert gas welding process. Here, the arc is maintained between a consumable electrode and the work piece in an inert gas atmosphere. The coiled electrode wire is fed by drive rolls as it melts away at the tip. Except for aluminum, a DC source is used with the consumable electrode as the positive terminal. [7]

Arc welding process plays an important contribution in manufacturing. Metal inert gas (MIG) welding is one of the most important arcs welding Process. MIG welding is a highly complex, multi-variable system, in which the variables affecting weld quality are not clearly known. Thus developing a model for making to prophesy of weld bead geometry has turned out to be non- trivial and number of approaches has been to exhibit to tackle the problem. In the present work, the input variables and responses for the MIG welding process have been investigated and different planning using grey relational analysis have been applied to prophesy the weld bead geometry. [3]

The requirements for quality products has led to the rapid advancement of today`s automated manufacturing environments. The quality of a product can be defined as the ability to fulfill the reasonable expectation and need set by the consumer. [8]

2 SCHEME OF INVESTIGATION

In order to maximize the quality characteristics, the present investigation has been made in the following sequence.

- Selection of base material.
- Identify the importance MIG welding process parameters.
- Find the upper and lower limits (i.e. range) of the identified process parameters.
- Select the orthogonal array (design of matrix).
- Conduct the experiments as per the selected orthogonal array.
- Record the quality characteristics (i.e. material properties).
- Find the optimum condition for maximizing the mechanical properties.
- Conduct the confirmation test.
- Identify the significant factors.
- Check the adequacy of the developed models.

3. GREY RELATIONAL ANALYSIS

3.1. DATA PREPROCESSING

Grey data processing must be performed before Grey correlation coefficients can be calculated. A series of various units must be transformed to be dimensionless. Usually, each series is normalized by dividing the data in the original series by their average. Let the original reference sequence and sequence for comparison be represented as $x_i^{(0)}$ and $x_i^{(k)}$, $i=1, 2, \dots, m$; $k=1, 2, \dots, n$, respectively, where m is the total number of experiment to be considered, and n is the total number of observation data. Data preprocessing converts the original sequence to a comparable sequence. Several methodologies of preprocessing data can be used in Grey relation analysis, depending on the characteristics of the original sequence. If the target value of the original sequence is “the-larger-the-better”, then the original sequence is normalized as follows.[2]

$$x_i^*(k) = \frac{x_i^{(0)}(k) - \min . x_i^{(0)}(k)}{\max . x_i^{(0)}(k) - \min . x_i^{(0)}(k)} \quad (1)$$

If the purpose is “the-smaller-the-better”, then the original sequence is normalized as follows

$$x_i^*(k) = \frac{\max . x_i^{(0)}(k) - x_i^{(0)}(k)}{\max . x_i^{(0)}(k) - \min . x_i^{(0)}(k)} \quad (2)$$

However, if there is “a specific target value” then the original sequence is normalized using.

$$x_i^+(k) = 1 - \frac{|x_i^{(0)}(k) - OB|}{\max. \left\{ \max. x_i^{(0)}(k) - OB, OB - \min. x_i^{(0)}(k) \right\}} \quad (3)$$

Where OB is the target value.

Alternatively, the original sequence can be normalized the simplest methodology that is the values of the original sequence can be divided by the first value of the sequence, $x_i^{(0)}(1)$.

$$x_i^+(k) = \frac{x_i^{(0)}(k)}{x_i^{(0)}(1)} \quad (4)$$

Where $x_i^{(0)}(k)$ is the original sequence, $x_i^+(k)$ the sequence after the data preprocessing, $\max. x_i^{(0)}(k)$ The largest value of $x_i^{(0)}(k)$, $\min. x_i^{(0)}(k)$: the smallest value of $x_i^{(0)}(k)$.

3.2. CALCULATION OF GREY RELATIONAL COEFFICIENT AND GREY RELATIONAL GRADES:

Following the data preprocessing, a Grey relational coefficient can be calculated using the preprocessed sequences. The Grey relational coefficient is defined as follows.

$$\gamma(x_0^+(k), x_i^+(k)) = \frac{\Delta_{\min.} + \zeta \Delta_{\max.}}{\Delta_{0i}(k) + \zeta \Delta_{\max.}}$$

$$0 < \gamma(x_0^+(k), x_i^+(k)) \leq 1 \quad (5)$$

Where $\Delta_{0i}(k)$ is the deviation sequence of reference sequence $x_0^+(k)$ and comparability sequence $x_i^+(k)$, namely?

$$\Delta_{0i}(k) = |x_0^+(k) - x_i^+(k)|, \quad \Delta_{\max.} = \max_{j \in i} \max_k |x_0^+(k) - x_j^+(k)|,$$

$$\Delta_{\min.} = \min_{j \in i} \min_k |x_0^+(k) - x_j^+(k)|,$$

ζ is the distinguishing coefficient, $\zeta \in [0,1]$

A Grey relational grade is a weighted sum of the Grey relational coefficients, and is defined as follows.

$$\gamma(x_0^+, x_i^+) = \sum_{k=1}^n \beta_k \gamma(x_0^+(k), x_i^+(k))$$

$$\sum_{k=1}^n \beta_k = 1 \quad (6)$$

Here, the Grey relational grade $\gamma(x_0^*, x_i^*)$ represents the level of correlation between the reference and comparability sequences. If the two sequences are identical, then the value of the Grey relational grade equals to one. The Grey relational grade also indicates the degree of influence exerted by the comparability sequence on the reference sequence.

Consequently, if a particular comparability sequence is more important to the reference sequence than other comparability sequences, the Grey relational grade for that comparability sequence and the reference sequence will exceed that for other Grey relational grades. The Grey relational analysis is actually a measurement of the absolute value of data difference between the sequences, and can be used to approximate the correlation between the sequences.

3.3 ANALYSIS OF VARIANCE (ANOVA)

Analysis of variance (ANOVA) and F-test (standard analysis) are used to analysis the experimental data as given follows. [7]

Notation:

Following Notation are used for calculation of ANOVA method

C.F. = Correction factor

T = Total of all result

n = Total no. of experiments

ST = Total sum of squares to total variation.

X_i = Value of results of each experiments ($i = 1$ to 16)

S_Y = Sum of the squares of due to parameter Y ($Y = A, B, C, D, E$)

NY_1, NY_2, NY_3, NY_4 = Repeating number of each level (1, 2, 3, 4) of parameter Y

XY_1, XY_2, XY_3, XY_4 = Values of result of each level (1, 2, 3, 4) of parameter Y

f_Y = Degree of freedom (D.O.F.) of parameter of Y

f_T = Total degree of freedom (D.O.F.)

f_e = Degree of freedom (D.O.F.) of error terms V_Y = Variance of parameter Y

S_e = Sum of square of error terms V_e = Variance of error terms

F_Y = F-ratio of parameter of Y S_Y' = Pure sum of square

C_Y = Percentage of contribution of parameter Y

C_e = Percentage of contribution of error terms

$CF = T^2/n$

$ST = \sum_{i=1}^{16} X_i^2 - CF$

$S_Y = (XY_{12}/NY_1 + XY_{22}/NY_2 + XY_{32}/NY_3 + XY_{42}/NY_4) - CF$

$f_Y = (\text{number of levels of parameter Y}) - 1$ $f_T = (\text{total number of results}) - 1$

$f_e = f_T - \sum f_Y$ $V_Y = S_Y/f_Y$ $S_e = ST - \sum S_Y$

$V_e = S_e/f_e$ $F_Y = V_Y/V_e$

$S_Y' = S_Y - (V_e * f_e)$ $P_z = S_Y'/ST * 100\%$

$P_e = (1 - \sum P_Y) * 100\%$

4. EXPERIMENTAL PROCEDURES

4.1 EXPERIMENTAL SETUP

Experiments were conducted MIG welding machine equipment which is shown in fig 1.

The MIG welding L&T, ZUPER ARC machine setup consist of machining base ,the equipments DC output source, Wire feed unit, Torch, Work return welding lead, Shielding gas supply, (normally from cylinder).power source have a Main supply line, on/off switch, Transformer,

Rectifier, Welding regulator. Most modern wire feed units control the wire feed speed via a DC motor and thruster control PCB to provide continuous control of Armature volts and hence RPM of motor. The MIG torch can be air cooled or water cooled and most modern air cooled torches have a single cable in which the welding wire slides through a liner. Gas flows around the outside of this liner and around the tube the liner sits in the power braid and trigger wires. MIG torch combination have a gas nozzle, contact tip, contact tip holder, liner, swan neck, trigger, and gun plug, trigger cables, current cable, gas hose. The shielding gas should also have a pronounced effect on the following aspects of the welding operation and the resultant weld. Arc characteristics, Mode of Metal Transfer, Penetration and Weld Head profile, Speed of Welding, Undercutting Tendency, and Cleaning Action Weld Metal Mechanical Properties. A basic position or starting point would be Aluminum – Argon, Magnesium – Helium, Copper Alloys – Argon – Helium Mix, Steel – Carbon dioxide not commonly used, Today, Argon-Carbon dioxide mix is preferred.



Figure 1: MIG welding machine setup

4.2 SELECTION OF MATERIAL

In this study two alloy steel plate of length 250 mm width 40 mm 1.2 mm thickness and height is equivalent to plate thickness made of Alloy steel which is a high carbon alloy steel with high degree of hardness and which rises the temperature of the tool tip to visible red heat. Ordinary high carbon and low alloys tool steels do not withstand the heating effect and readily lose hardness. But high speed steels have the property to withstand this heating effect without losing hardness. So called high speed steels are of composition that have good wear resistance and retain their hardness of high temperature. A superior brand of high speed steel has the following composition as per ISS Carbon (0.70%), Tungsten (18.00%), Chromium (4.00%), and Vanadium (1.00%).

4.3 RECORD OF QUALITY CHARACTERISTICS

To evaluate the quality of MIG welds measurement of weld pool geometry are performed. In this study the bead width, bead height, penetration and heat affected zone (HAZ) of weld pool are used to describe

the weld pool geometry measured by Bridge cam gauge (BCG). These parameters measured accurately and one time measured by (BCG).

Tensile specimen of necessary dimension as per ASTM E8M were separated out from welding coupon plates and test were measured on 400 KN computer control universal testing machine. The specimen loaded at the rate of 1.5 KN/min as per ASTM specification. So that tensile specimen under goes deformation. The specimen finally fails after necking and load vs displacement was recorded. The tensile property higher the better quality characteristic.

4.4 SELECTION OF THE MIG WELDING PARAMETERS AND THEIR LEVELS

In this study, the experimental plan has five variables, namely, Wire diameter, Welding current, Arc voltage, Welding speed, and Gas flow rate. On the basis of preliminary experiment conducted by using one variable at a time approach, the feasible range for the welding parameters was defined by the Wire diameter (0.8-1.2mm), Welding current (80-110amp), Arc voltage (18-19.5VOLT), Welding speed (45-55cm/min), Gas flow rate (10-15ltr/min). In the MIG welding parameters were selected, shown in Table-1.

Table 1: Parameters and their levels

Notation	Process Parameter	Level 1	Level 2	Level 3	Level 4
A	Wire diameter (mm)	0.8	0.9	1	1.2
B	Welding current (amp)	80	90	100	110
C	Arc voltage (volt)	18	18.5	19	19.5
D	Welding speed (cm/mm)	45	48	51	55
E	Gas flow rate (let/min)	10	13	14	15

5. EXPERIMENTAL DESIGN

The application of design-of-experiments (DOE) to demand as of right anxious planning, best ground-plan of the experiment and table shown. The choose design matrix based on Taguchi L16 (45) orthogonal array consist 16 set of code condition and the experimental result for the response Tensile strength, Bead width, Bead height, penetration, and heat affected zone (HAZ) in process parameter. In the present study there 12 degree of freedom owing to the four level welding parameters. While the reciprocal action between the parameters is neglected. Once the DOF are known the next step is choose an appropriate orthogonal array. The DOF for the orthogonal array should be greater than or at least equal to those process parameters. In this study an L16 orthogonal array is used because it has 15 degree of freedom in the welding parameters. The experiment output for the process parameter is shown in Table 2.



Figure 2 :Work piece of steel alloy

Table 2. Experimental layout using L16 orthogonal array

Experiment No.	A	B	C	D	E
1	1	1	1	1	1
2	1	2	2	2	2
3	1	3	3	3	3
4	1	4	4	4	4
5	2	1	2	3	4
6	2	2	1	4	3
7	2	3	4	1	2
8	2	4	3	2	1
9	3	1	3	4	2
10	3	2	4	3	1
11	3	3	1	2	4
12	3	4	2	1	3
13	4	1	4	2	3
14	4	2	3	1	4
15	4	3	2	4	1
16	4	4	1	3	2

5.1 EXPERIMENTAL RESULTS

Table 3. Experimental results for steel alloy

Experiment No.	Tensile strength (N/mm ²) Larger is better	Bead width (mm) Smaller is better	Bead height (mm) Smaller is better	Penetration (mm) Larger is better	HAZ (mm) Smaller is better
1	260.12	8.1	0.251	1.263	5.621
2	262.17	8.19	0.259	1.264	5.72
3	271.16	8.61	0.273	1.277	5.8
4	269.27	8.5	0.26	1.278	5.77
5	265.71	8.43	0.251	1.273	5.765
6	272.18	8.65	0.275	1.288	5.806
7	252.17	7.19	0.203	0.985	3.868
8	272	8.61	0.281	1.291	5.996
9	257.19	7.21	0.21	1.05	4.38
10	262.11	8.1	0.235	1.212	5.72
11	281.16	8.91	0.294	1.306	6.127
12	277.91	8.77	0.288	1.298	6.099
13	261.33	8.05	0.231	1.239	5.712
14	271.16	8.51	0.271	1.281	5.937
15	255.34	7.05	0.21	0.998	4.367
16	267.14	8.43	0.255	1.235	5.766

Table 4. Preprocessed data results for steel alloy

Experiment No.	Tensile strength	Bead width	Bead height	Penetration	HAZ
1	0.274	0.435	0.225	0.866	0.223
2	0.344	0.387	0.183	0.869	0.18
3	0.655	0.161	0.109	0.909	0.144
4	0.589	0.22	0.178	0.912	0.158
5	0.467	0.258	0.225	0.897	0.16
6	0.69	0.139	0.099	0.943	0.142
7	0	0.924	1	0	1
8	0.684	0.161	0.068	0.953	0.057
9	0.173	0.913	0.439	0.202	0.773
10	0.342	0.435	0.308	0.707	0.18
11	1	0	0	1	0
12	0.887	0.075	0.031	0.975	0.012
13	0.315	0.462	0.329	0.791	0.183
14	0.655	0.215	0.12	0.922	0.084
15	0.109	1	0.439	0.04	0.779
16	0.516	0.258	0.204	0.778	0.159

Table 5. Grey relational coefficient for steel alloy

Experiment No	Tensile strength	Bead width	Bead height	Penetration	HAZ
1	0.645	0.534	0.689	0.366	0.691
2	0.592	0.563	0.732	0.365	0.735
3	0.432	0.756	0.821	0.354	0.776
4	0.459	0.694	0.737	0.354	0.759
5	0.517	0.659	0.689	0.357	0.757
6	0.42	0.782	0.834	0.346	0.778
7	1	0.351	0.333	1	0.333
8	0.422	0.756	0.88	0.344	0.897
9	0.742	0.353	0.532	0.712	0.892
10	0.593	0.534	0.618	0.414	0.735
11	0.333	1	1	0.333	1
12	0.36	0.869	0.941	0.338	0.976
13	0.613	0.519	0.603	0.387	0.732
14	0.432	0.699	0.806	0.351	0.856
15	0.821	0.333	0.532	0.925	0.39
16	0.492	0.659	0.71	0.391	0.758

Table 6. Grey relational grade for steel alloy

Experiment No.	A	B	C	D	E	Grey relational grade
1	1	1	1	1	1	0.585
2	1	2	2	2	2	0.597
3	1	3	3	3	3	0.627
4	1	4	4	4	4	0.6
5	2	1	2	3	4	0.595
6	2	2	1	4	3	0.632
7	2	3	4	1	2	0.603
8	2	4	3	2	1	0.659
9	3	1	3	4	2	0.546
10	3	2	4	3	1	0.578
11	3	3	1	2	4	0.733
12	3	4	2	1	3	0.696
13	4	1	4	2	3	0.57
14	4	2	3	1	4	0.628
15	4	3	2	4	1	0.6
16	4	4	1	3	2	0.602

Table 7. Response Table for grey relational for steel alloy

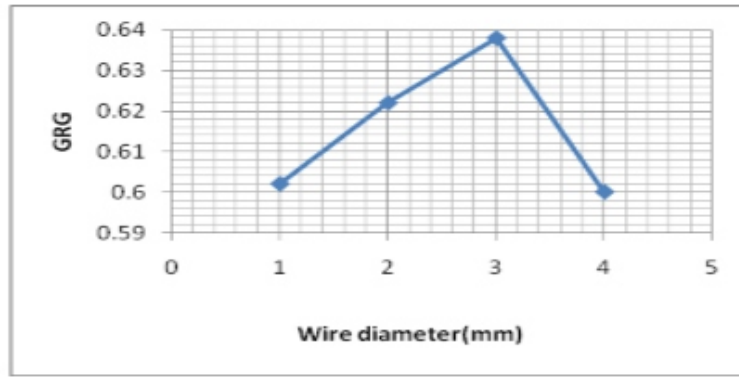
Levels	Factors				
	A	B	C	D	E
1	0.62	0.574	0.638	0.628	0.605
2	0.622	0.608	0.622	0.639	0.587
3	0.638	0.64	0.615	0.6	0.631
4	0.6	0.639	0.587	0.594	0.639

5.2 ANALYSIS OF VARIANCE (ANOVA)

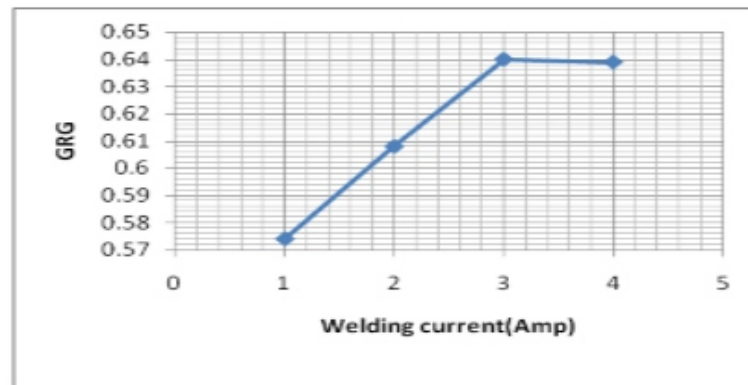
Analysis of variance (ANOVA) was introduced by Sir Ronald Fisher. The purpose of the analysis of variance (ANOVA) is to investigate which design parameters significantly affect the quality characteristic.

Table 8. Analysis of variance (ANOVA) and F-test for steel alloy

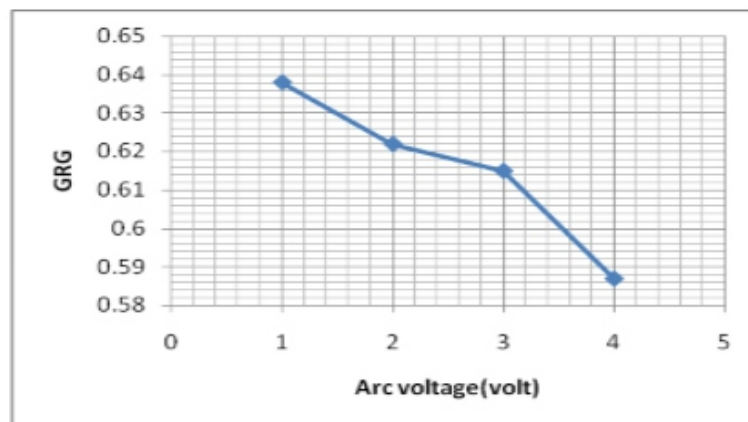
Factor	DOF	Sum of squares	Mean variance	F-ratio	Sz	Contribution (%)
A	3	0.002	0.00066	0.00066	0.002	6.896
B	3	0.01	0.0033	0.0033	0.01	34.483
C	3	0.003	0.001	0.001	0.003	10.345
D	3	0.004	0.0013	0.0013	0.004	13.793
E	3	0.005	0.0016	0.0016	0.005	17.241
Error	0	0.005				17.242
Total	15	0.029	0.0078			100



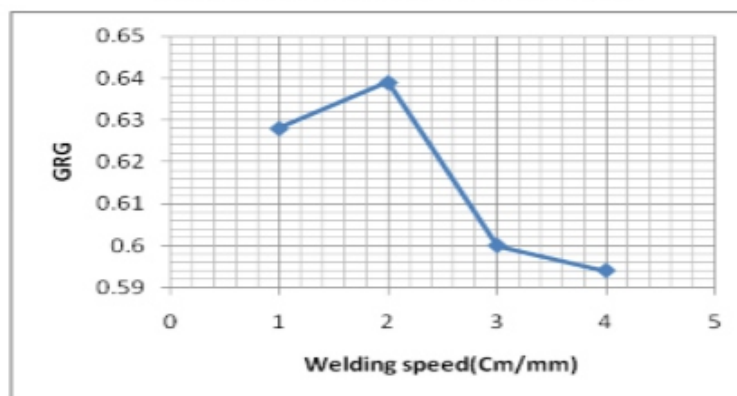
Graph between GRG and wire diameter



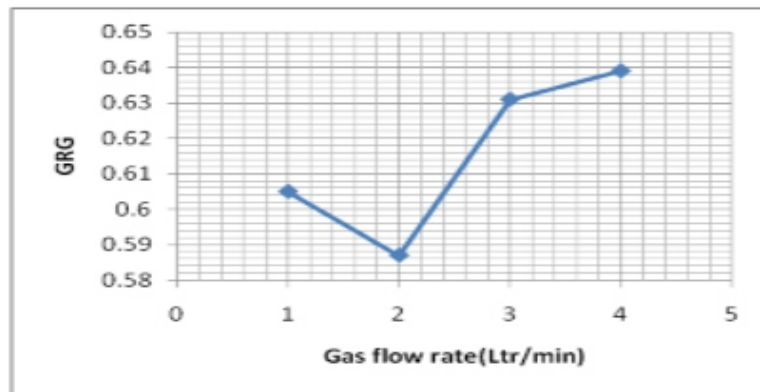
Graph between GRG and welding current



Graph between GRG and Arc voltage



Graph between GRG and welding speed



Graph between GRG and Gas flow rate

Figure 3: Influence Performances For Steel Alloy Of Process Parameters On Multiple

RESULT AND DISCUSSION

After identifying the most influential parameters, the final phase is to verify the Tensile strength, Bead width, Bead height, Penetration and Heat affected zone by conducting the confirmation experiments. The A3B3C1D2E4 is an optimal parameter combination for steel alloy of the MIG welding process via the Grey relational analysis. Therefore, the condition A3B3C1D2E4 of the optimal parameter combination of the MIG welding process was treated as a confirmation test. If the optimal setting for steel alloy with a Wire diameter 1mm, Welding current 100 A, Arc voltage 18 V, Welding speed 48 cm/min, and Gas flow rate 15 ltr/min is used, the final work piece gives the Bead width (6.05mm), Bead height (0.103mm) and HAZ (2.868mm) minimum, Tensile strength (282.16N/mm²) and Penetration (2.306mm) is maximum.

CONCLUSION

In the present study, Taguchi optimization technique pair with grey relational analysis has been adopted for evaluating parametric complex to carry out acceptable Tensile strength and Penetration higher is better. Bead width, Bead height and Heat affected zone (HAZ) lower is better of the alloy steel element to acquired by using Metal inert gas welding. After identify the predict optimal parameter setting with the help of (ANOVA) the most significant factor also found in this case welding current is having maximum percentage contribution. So it is most significant factor in this result.

REFERENCES

- [1] S.V. Sapakal1, M.T. Telsang2 “parametric optimization of MIG welding using taguchi design method”. Vol. 1/Issue 4th/july-sept, 2012/28-30
- [2] Sukhomany Pal. Santosh K. Malviya. Surjya K. Pal. Arun K. Samantaray, “Optimization of quality characteristics parameters in a pulsed metal inert gas welding process using grey-based Taguchi method” (2009)44:1250-1260
- [3] A.S. shahi, S. pandey “ Modeling of the effects of welding condition on dilution of stainless steel cladding produced by gas metal arc welding procedures.” *Journals of materials processing technology* 196.PP, 339-344, 2008.
- [4] K. Y. Benyounis, A.G. Olabi, “optimization of different welding process using statistical and numerical approaches –A reference guide” *Advance in engineering software* 39 (2008) 483-496
- [5] Saurav Datta, Ashish Bandyopadhyay, Pradeep Kumar Pal. Grey based Taguchi method for optimization of bead geometry in submerged arc bead-on-plate welding. *International journal of Advance Manufacturing Technology* (2008) 39:1136-1143.

-
-
- [6] J.P. Ganjigatti, Dilip Kumar Pratihari, A. Roy Choudhury, "Global versus cluster-wise regression analysis for prediction of bead geometry in MIG welding process" *Journal of Materials processing Technology* 189 (2007)352-366.
- [7] N.B. Mostafa, M.N. Khajavi, "Optimization of welding parameters for weld penetration in FCAW" *Achievements in material and Manufacturing Engineering* Vol. 16 ISSUE 1-2 May-June 2006.
- [8] V.M. Radhakrishnan, *welding technology & design (second edition 2005)*, New Age International Publishers, New Delhi.
- [9], Ross, P.J, *Taguchi Techniques for quality engineering, second edition, 2005, TMH publishing, New Delhi.*
- [10] I. S. Kim, C.E. Park, K.D.V. Prasad, Yarlagadda, *A study on the prediction of process parameter in the Gas Metal Arc Welding (GMAW) of mild steel using Taguchi Methods, Mater. Sci. Forum* (2003) 235-238.
- [11] N. Murugan, R.S. parmar, "Effects of MIG process parameters on the geometry of the bead in the automatic surfacing of the stainless steel," *Journal of material processing technology, vol 41, PP. 381-398, 1994.*
- [12] H.J. Park, D.C. Kim, M.J. Kang, S. Rhee, "Optimization of the wire feed rate during pulse MIG welding of Al sheets" *Journals of Achievements in materials and Manufacturing Engineering Volume 27, by international OCSCO world.*
- [13] P. Sathiya, Swati, V. Manaswini, Anubha Singh Bhadauria and Snigdha Lakra, "Optimizing The gas metal arc welding parameter of super Austenitic Stainless steel by Grey Based Taguchi,s Method".

Principal Stress Analysis of Luffing Jib using Solid Works-12

Atul shanker suman* Jyoti vimal, Vedansh chaturvedi****

*Research Scholar, Department of Mechanical Engineering, Madhav Institute of Technology & Science, Gwalior, Madhya Pradesh

**Asst. Professor, Department of Mechanical Engineering, Madhav Institute of Technology & Science, Gwalior, Madhya Pradesh

ABSTRACT

Now-a-days, the tower crane is a basic need in the infrastructure field. The loading & unloading work is performing by the tower crane. Mobile tower crane is a type of tower crane which is used for the purpose of easy handing of material on different location of work station by its portable function. Failure of the tower crane may be occur during due to failure of, its design. This study focus on the prevention of crane damage which occur due to heavy load.

In this study, by using the SOLID WORKS-12 software the crane parts material which is made by plain carbon steel is modeled one-by-one, with specific dimensions. Afterwards the principal stress distribution analysis done by SOLID WORKS-12 software. As the conclusion the safe design of mobile tower crane for 900 at a load of 800 kg on a different length of jib is recommended.

Key words: Mobile tower crane (luffing jib), plain carbon steel, SOLIDWORK-12.

INTRODUCTION

Mobile tower crane are the self erecting/self folding tower crane. Operation can be easily affected by a single operator, through a remote control pod. This crane is mounted on a towable type trailer with compact dimensions for easy transportation. To minimize the dead weight for long distance transportations the counter weight box is designed with trap doors to enable general ballast use as a counter weight. The chassis design enables a short turning radius & easy positioning. Stabilizers are out & down type and can be reiterated into the lower chassis to satisfy the road clearance codes. An optional prime mover with a built in 20KVA generator makes. Mobile tower crane totally independent of any outside electric source and have separate carrier vehicle. The crane uses only a part of the power & generator can be used for other site equipment like mixers, vibrators & job site lighting system. Some mobile tower crane is controlled by a remote. This facilitates the operator position himself in such way that he can see both picking as well as dumping points for precise load & positioning.

In this study, a mobile tower crane is modeled in 3D using SOLIDWORK-12 computer software. Then, the generated components are meshed in SOLID WORKS-12 software. The meshed components are mounted on each other and the meshed model of the tower crane is obtained. Finite element analysis is accomplished considering the load combination in FEM norms.

MAIN BODY

The raw material used for construct the main body of the mobile tower crane is plain carbon steel. Carbon steel is by far the most widely used kind of steel. The properties of carbon steel depend primarily on the amount of carbon it contains. Most carbon steel has a carbon content of less than 1%. Carbon steel is made into a wide range of products, including structural beams, car bodies, kitchen appliances, and

cans. In fact, there are 3 types of plain carbon steel and they are low carbon steel, medium carbon steel, high carbon steel, and as their names suggests all these types of plain carbon steel differs in the amount of carbon they contain. Indeed, it is good to precise that plain carbon steel is a type of steel having a maximum carbon content of 1.5% along with small percentages of silica, sulphur, phosphorus and manganese.

The following property of the plane carbon steel is used.


Model Reference	Properties	
	<u>Material property</u>	
	Material name	Plain Carbon Steel
	Yield strength	2.20594e+008 N/m ²
	Tensile strength:	3.99826e+008 N/m ²
	Elastic modulus	2.1e+011 N/m ²
	Poisson's ratio:	0.28
	Mass density	7800 kg/m ³
	Shear modulus	7.9e+010 N/m ²
	Thermal expansion coefficient	1.3e-005 /Kelvin

Figure 1: Properties of plain carbon steel

The specification of the tower crane is;

S.N.	Height	Reach	Capacity
Horizontal jib position	23 meter	7.5-25meters	2500K gs.-800K gs.
Raised jib position	23 meter	7.5-25meters	2500K gs.-800K gs.

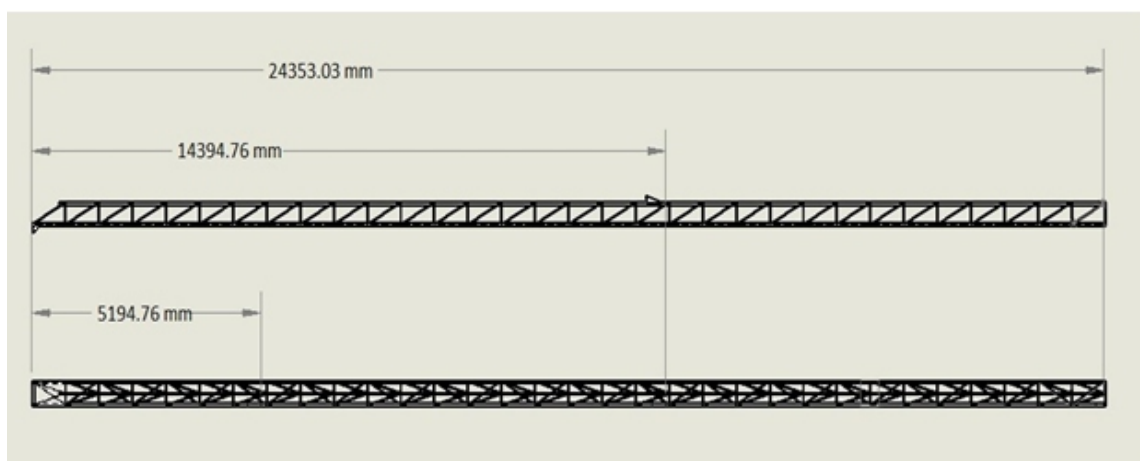


Figure: 2 Top & front view (load is applied on a different length)

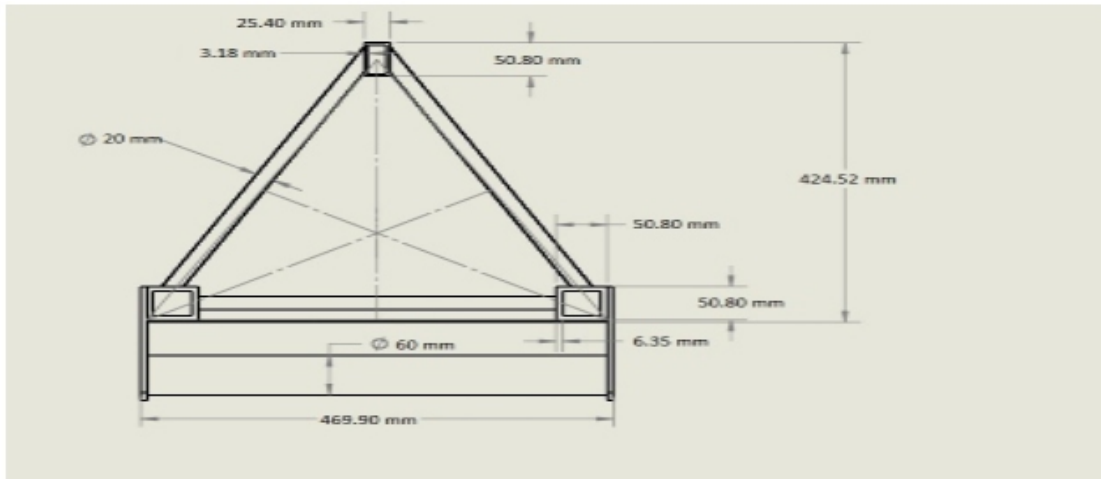


Figure 3: side view of the luffing jib.

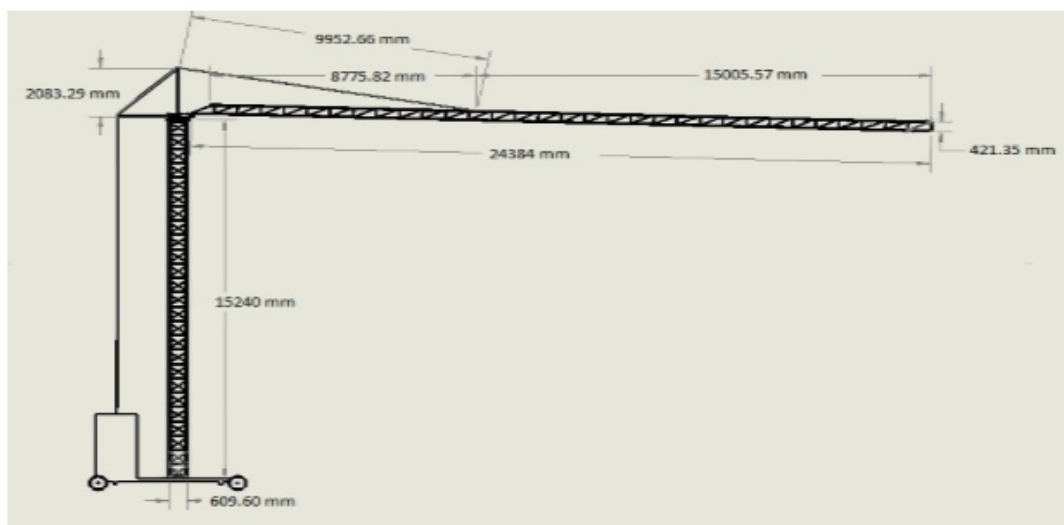



Figure 4: final view of the mobile tower crane

RESULT & DISCUSSION

a). Principal stress on a different axis of the jib (Load applied on the beginning point)

Solid Bodies		
Model reference	Treated As	Volumetric Properties
	Solid Body	<p>Mass:668.154 kg</p> <p>Volume:0.0856608 m³</p> <p>Density:7800 kg/m³</p> <p>Weight:6547.91 N</p>

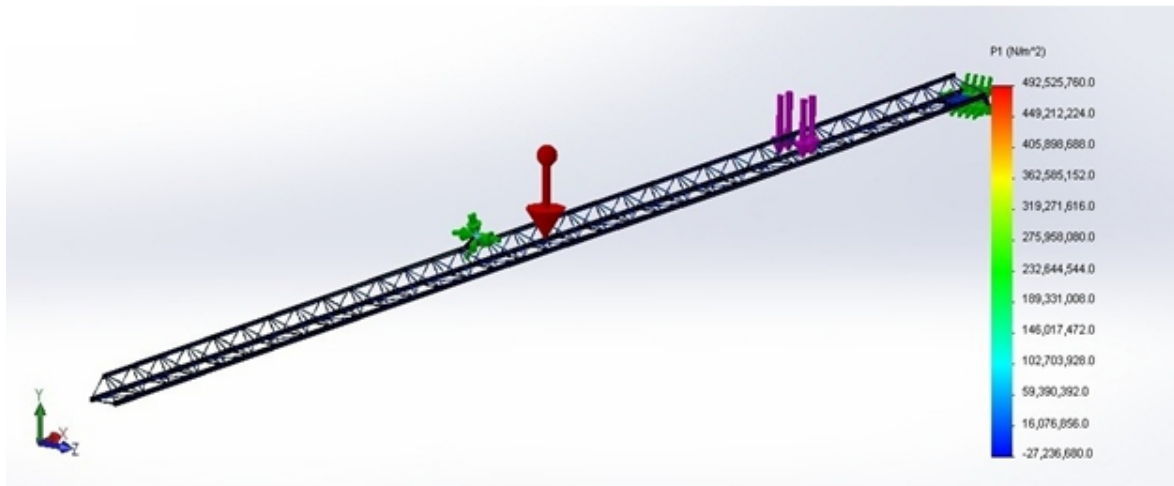


Fig. a (1)

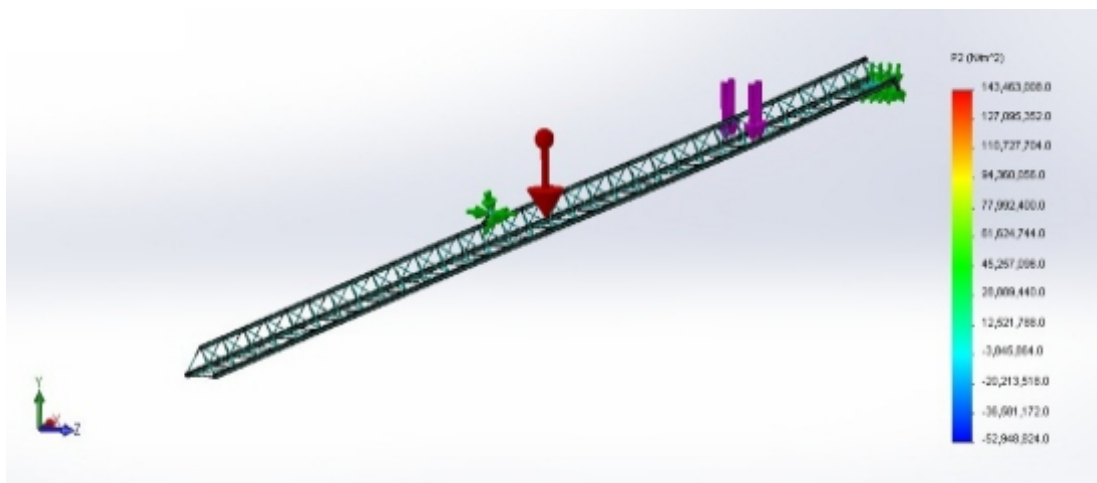


Fig. a (2)

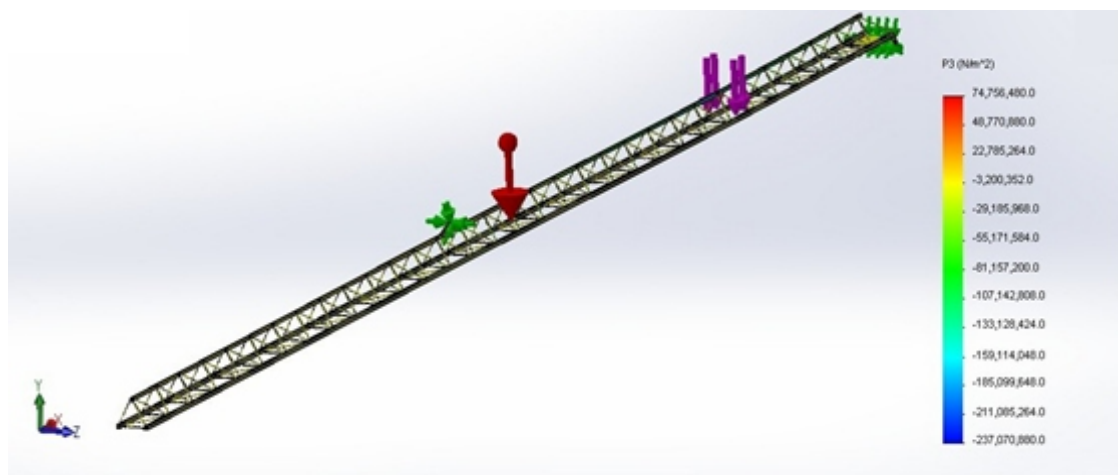


Fig. a (3)

The above result showed the principal stress distribution for an applied load of 800 kg at a distance 5194.76 mm from fixed and hinge point at the beginning. The three mutual perpendicular principal stresses on their principal axis, which are P1, P2, P3 respectively. The P1, P2, P3 are lie on the X-axis, Y-axis and Z-axis. In the solid works analysis the positive sign convention indicate the tensile stress on the


body where as the negative sign convention indicate the compressive stress on the body. If result having both sign convention (positive & negative), so its mean that the body is in pure banding.

By the solid works analysis the result shown that [fig a (1)] the maximum principal stress (P1) which is lie on the X-axis is 492,525,760.0 N/m² & the minimum principal stress is -27,236,680.0 N/m².

Now on the second [fig a (2)] result analysis shows the maximum principal stress (P2) which is lie on the Y-axis, is 143,463,008 N/m² & the minimum principal stress is -52,948,824.0 N/m².

And the third [fig a (3)] result analysis shows the maximum principal stress (P3) which is lie on the Z-axis, is 74,756,480.0 N/m² & the minimum principal stress is -237,070,880.0 N/m².

b). Principal stress on a different axis of the jib (Load applied on the middle point)

Solid Bodies		
Model reference	Treated As	Volumetric Properties
	Solid Body	<p>Mass:668.154 kg</p> <p>Volume:0.0856608 m³</p> <p>Density:7800 kg/m³</p> <p>Weight:6547.91 N</p>

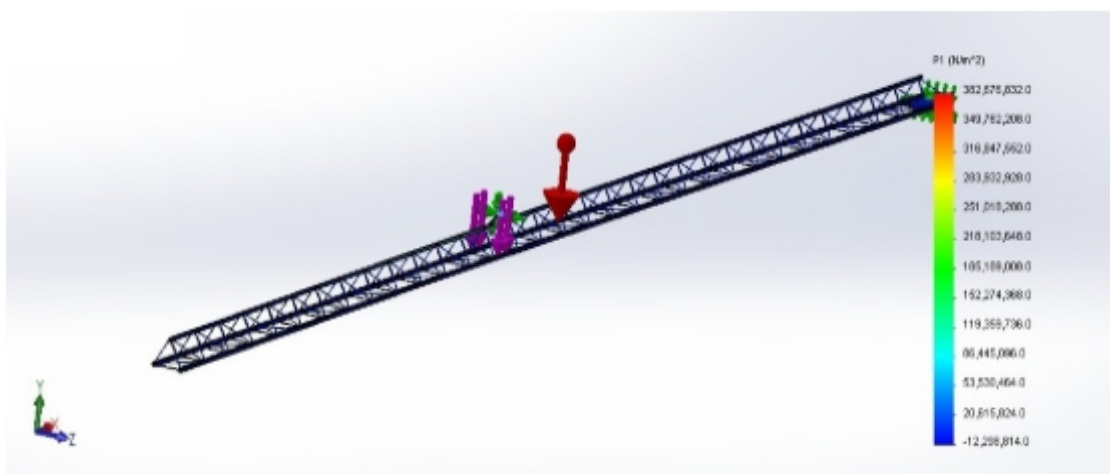


Fig. b (1)

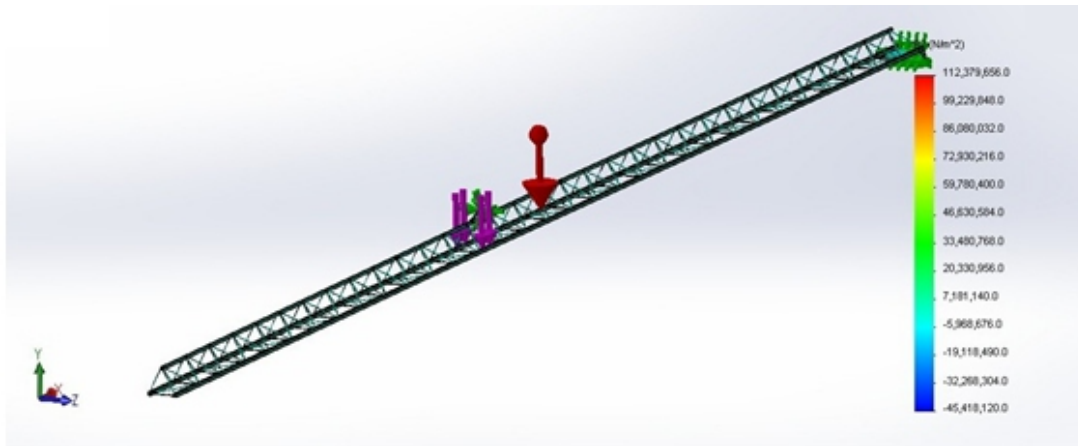


Fig. b (2)

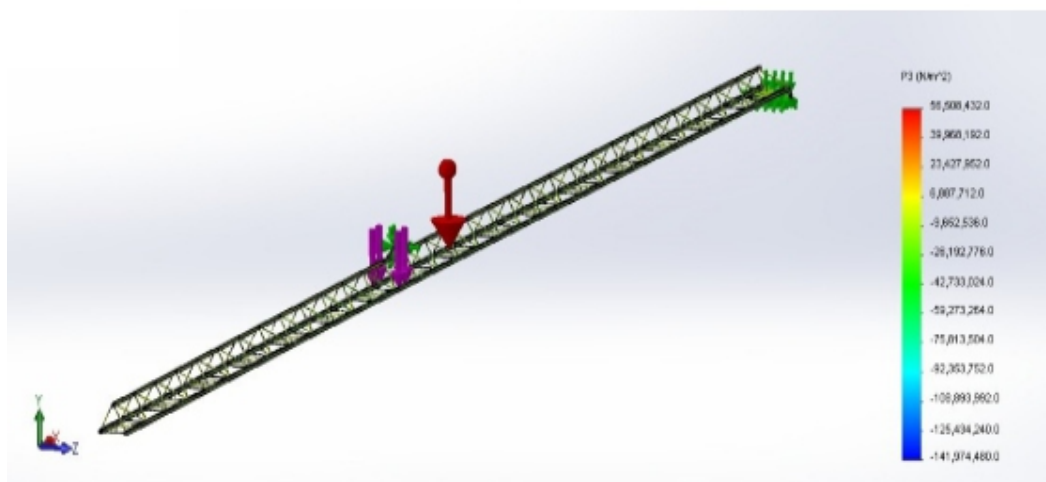



Fig. b (3)

The next analysis principal stress on a different axis of the jib (Load applied on the middle point) showed that principal stress distribution for an applied load of 800 kg at a distance 14394.76 mm from fixes and hinge point at the beginning. The three mutual perpendicular principal stresses on their principal axis, which is P1 P2 P3 respectively. The P1 P2 P3 are lie on the x axis y axis and z axis.

By the solid works analysis the result shown that [fig b (1)] the maximum principal stress (P1) which is lie on the X-axis is 382,676,832.0 N/m² & the minimum principal stress is - 12,298,814.0 N/m².

Now on the second [fig b (2)] result analysis shows the maximum principal stress (P2) which is lie on the Y-axis, is 112,379,656.0 N/m² & the minimum principal stress is -45,418,120.0 N/m². And the third [fig b (3)] result analysis the maximum principal stress (P3) which is lie on the Z- axis, is 56,508,432.0 N/m² & the minimum principal stress is -141,974,480.0 N/m².

c). Principal stress on a different axis of the jib (Load applied on the last point)

Solid Bodies		
Model reference	Treated As	Volumetric Properties
	Solid Body	<p>Mass:668.154 kg</p> <p>Volume:0.0856608 m³</p> <p>Density:7800 kg/m³</p> <p>Weight:6547.91 N</p>

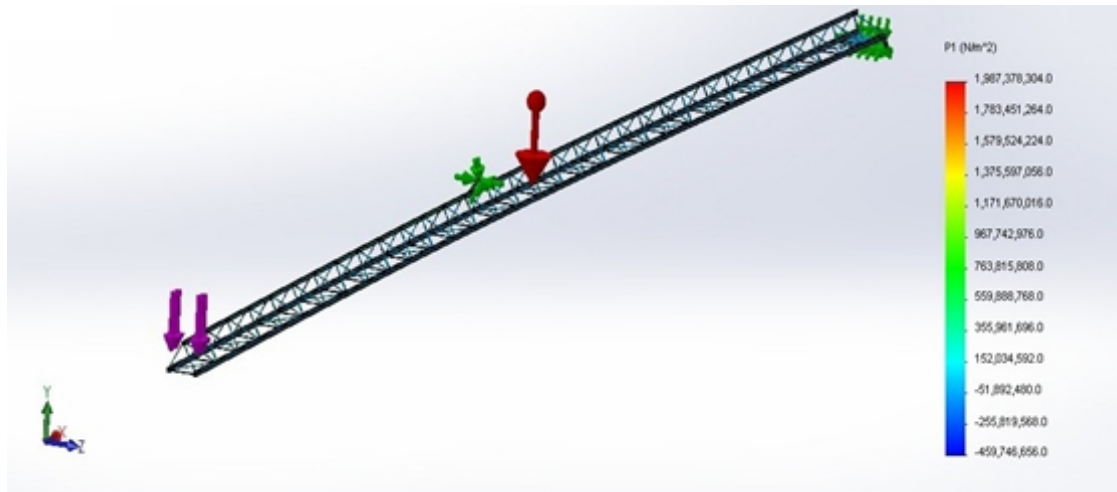


Fig. c (1)

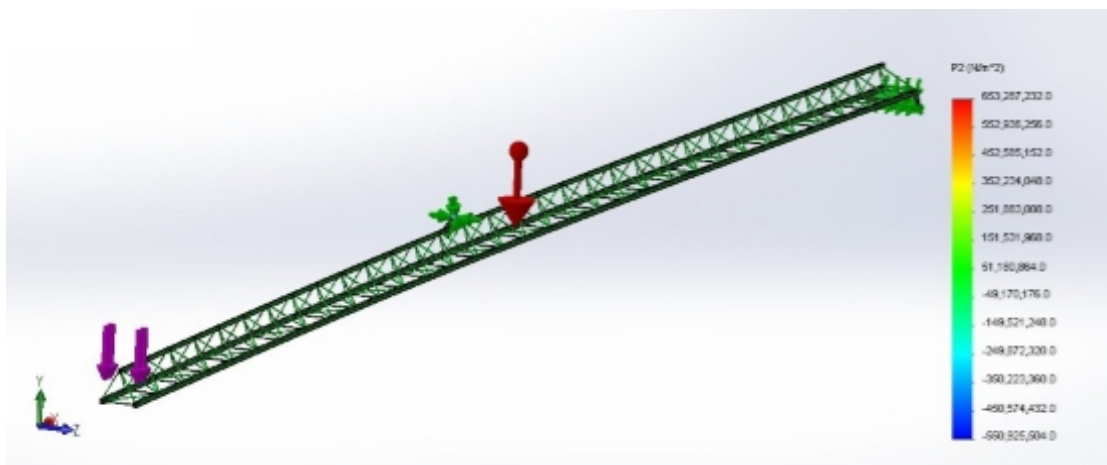


Fig. c (2)

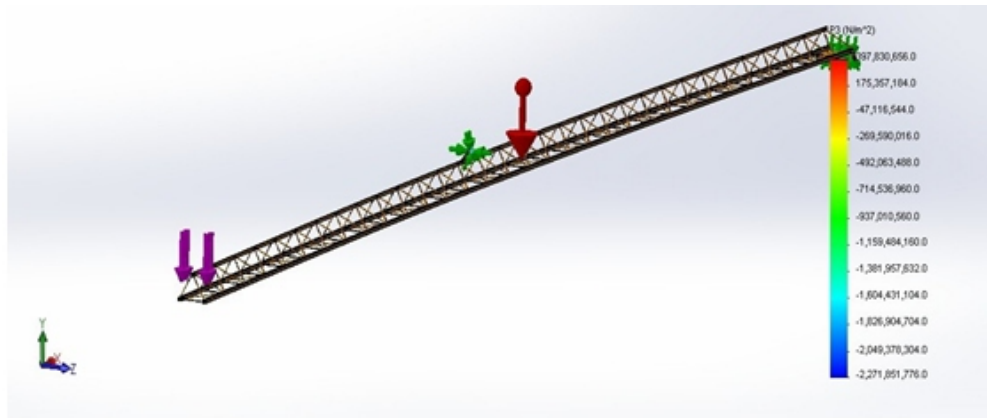


Fig. c (3)

The next analysis principal stress on a different axis of the jib (Load applied on the last point) showed that principal stress distribution for an applied load of 800 kg at a distance 24353.03 mm from fixed and hinge point at the beginning. The three mutual perpendicular principal stresses on their principal axis, which are P1, P2, P3 respectively. The P1, P2, P3 are located on the x, y, and z axes.

By the SolidWorks analysis the result shown that [fig b (1)] the maximum principal stress (P1) which is located on the X-axis is 1,987,378,304.0 N/m² & the minimum principal stress is -459,746,656.0 N/m².

Now on the second [fig b (2)] result analysis the maximum principal stress (P2) which is located on the Y-axis, is 653,287,232.0 N/m² & the minimum principal stress is -550,925,504.0 N/m².

And the third [fig b (3)] result analysis the maximum principal stress (P3) which is located on the Z-axis, is 397,830,656.0 N/m² & the minimum principal stress is -2,271,851,776.0 N/m².

CONCLUSION

Analysis result of luffing jib tower crane reveals that the compressive stress is maximum in Z-direction at all applied load condition and analysis of the diagrammed shown that the generation of compressive stress is maximum in the luffing jib (which shows by the negative value of principal stress) as compared to tensile (which shows by the positive principal stress).

So in loading and unloading by the luffing jib the factor of safety in Z-direction should be highly taken into consideration.

REFERENCE

1. Kazuya ITOH, Naoaki SUEMASA, Satoshi TAMATE 2004 "DYNAMIC LOADING TEST FOR PILE SUPPORTED TOWER CRANE IN SOFT CLAY" 13th World Conference On Earthquake Engineering Vancouver, B.C., Canada August 1-6, 2004 Paper No. 820
2. Lanfeng Yu, 2007 "CALCULATION METHOD AND CONTROL VALUE OF STATIC STIFFNESS OF TOWER CRANE" Journal Of Mechanical Science And Technology 22 (2008) 829~834
3. Ismail Gerdemeli, Serpil Kurt, Okan Delikatlas, "FINITE ELEMENT ANALYSIS OF THE TOWER CRANE" Trends In The Development Of Machinery And Associated Technology, TMT2010, Mediterranean, 11-18 September 2010.
4. Nenad D. Zmic, Srđan M. Bosnjak, Valda M. Gasic, 2011 "FAILURE ANALYSIS OF THE TOWER CRANE COUNTERJIB" Procedia Engineering 10 (2011) 2238~2243.
5. Vivian W.Y. Tam, Ivan W.H. Fung 2010 "TOWER CRANE SAFETY IN THE CONSTRUCTION INDUSTRY" Safety Science 49 (2011) 208~215.

Wear Rate of (Aluminium) AL-6061 on Different Loads

*** Rahul Jaiswal**

M.Tech, B.Tech, Student/Scholar Maharishi University of Information
Technology, Lucknow.

ABSTRACT

Wear is the important factor for various applications in automobile and aeronautical industries. Various researches are going on to improve the wear by either alloying the material or using the composite material. Wear is related to interactions between surfaces and more specifically the removal and deformation of material on a surface as a result of mechanical action of the opposite surface. The research work summarized in this thesis present an experimental investigation on the effect of abrasive wear rate of the material Al-6061 alloy on various load. The experiment was carried out in the laboratory using an experimental set up for the analyzing the wear rate of selected material. The experiment for analyzing the wear rate conducted on various load as well as various orientation against grinding disc. Here we study the working life of an engineering component is expired when dimensional losses exceed the specified tolerance limits. The abrasive wear behavior of selected material is analyzing at different loads and four different orientations. In the above paper I have analyzed the abrasive wear of selected material, which shows the estimated life of said material.

Copyright © 201x International Journals of Multidisciplinary Research Academy. All rights reserved.

OBJECTIVE OF THE STUDY:

To analyzing the wear rate for different load and different orientation for ma selected material during abrasive wear rate. This shows the material life against the selected load.

INTRODUCTION-

In materials science, wear is erosion or sideways displacement of material from its "derivative" and original position on a solid surface performed by the action of another surface.

Wear is related to interactions between surfaces and more specifically the removal and deformation of material on a surface as a result of mechanical action of the opposite surface Rabinowicz, E 1995 [1]. The need for relative motion between two surfaces and initial mechanical contact between asperities is an important distinction between mechanical wear compared to other processes with similar outcomes. Williams, J.A.2005[2].

The definition of wear may include loss at the interface between two sliding surfaces. However, plastic deformation such as yield stress is excluded from the wear definition if it doesn't incorporates a relative sliding motion and contact against another surface despite the possibility for material removal, because it then lacks the relative sliding action of another surface. Impact wear is in reality a short sliding motion where two solid bodies interact at an exceptional short time interval. Previously due to the fast execution, the contact found in impact wear was referred to as an impulse contact by the nomenclature. Impulse can be described as a mathematical model of a synthesized average on the energy solids in opposite converging contact. Cavitations wear is a form of wear where the erosive medium or counter-body is a fluid. Corrosion may be included in wear phenomenon, but the damage is amplified and performed by chemical reactions rather than mechanical action.

Wear can also be defined as a process where interaction between two surfaces or bounding faces of solids within the working environment results in dimensional loss of one solid, with or without any actual decoupling and loss of material. Aspects of the working environment which affect wear include loads and features such as unidirectional sliding, reciprocating, rolling, and impact loads, speed, temperature, but also different types of counter-bodies such as solid, liquid or gas and type of contact ranging between single phase or multiphase, in which the last multiphase may combine liquid with solid particles and gas bubbles.

When surfaces in contact move relative to each other, the friction between the two surfaces converts kinetic energy into heat. This property can have dramatic consequences, as illustrated by the use of friction created by rubbing pieces of wood together to start a fire. Kinetic energy is converted to heat whenever motion with friction occurs, for example when a viscous fluid is stirred. Another important consequence of many types of friction can be wear, which may lead to performance degradation and/or damage to components. Friction is the component of science of tribology.

Friction is not a fundamental force but occurs because of the electromagnetic forces between charged particles which constitute the surfaces in contact. Because of the complexity of these interactions, friction cannot be calculated from first principles, but instead must be found empirically. Some factors affecting wear rate such as Coefficient of friction, Specific energy of material, Material removal rate. This includes the width of the grinding wheel, Depth of cut, Feed rate of the specimen, power unit-torque & speed. In recent decades, aluminum alloy based metal matrix are gaining important role in several engineering applications. Al6061 alloy has been used as the matrix material because of its good formability, excellent mechanical properties and manufacturing properties. Wide spectrum of the applications in the commercial and industrial sectors.

Chemical composition of the Al6061 alloy are as

Elements	Cu	Mn	Mg	Si	Fe	Cr	Ti	Zn
Wt%	0.15-0.40	0.15	0.8-1.2	0.4-0.8	0.7	0.04-0.35	0.15	0.25

Aluminum alloy(Al6061)- By the adopting the suitable treatment, mechanical properties of wear resistance of Al composites can be improved. Studying wear is characterized by many different aspect and it is mostly influenced by the complexity of materials interaction on a functional surface as well as by operation conditions. In machine element, there are gradual wear in the result of friction. Therefore, we have to search for the possibilities to prevent it thus extending the technical life of a component.

LITERATURE REVIEW-

- **Chang Chongyi** Wang Chenggu and Jin Ying 2010[14] They conducted their study on numerical method to predict wheel/rail profile evolution due to wear. A wheel/rail profile wear prediction methodology was developed and applied to the wheel/rail disc test about the wear of flange and gauge. Three-dimensional nonlinear finite element dynamic analysis code ABAQUS was also used in the simulation of wheel/rail disc rolling contact process. The simulation results are compared with measurements of laboratory wear test and the effectiveness of the wear prediction methodology was verified.

-
- **Dharma R. Maddala, Arif Mubarak and Rainer J. Hebert 2010[15]** conducted study on Sliding wear behavior of Cu₅₀Hf_{41.5}Al_{8.5} bulk metallic glass. Sliding wear behavior of a copper- based bulk metallic glass (Cu₅₀Hf_{41.5}Al_{8.5}) was investigated for both as-cast and annealed samples. The wear resistance increased during isothermal annealing near the glass transition temperature. Nano crystals developed during the annealing for annealing times up to 300 min. A linear relation between hardness and wear resistance was observed during the early stages of devitrification, but at longer annealing times the wear resistance increased less than the hardness.
 - **H.C. How and T.N. Baker 1997[18]** In their investigation of wear behavior of Al6061-saffil fiber, concluded that saffil are significant in improving wear resistance of the composite.
 - **Liang Y. N. et. al. 1995 [19]** Reported that the MMCs containing SiC particles exhibit improved wear resistance.
 - **Basavarajappa S., et. al. 2005 [20]** Stated that the micro structural characteristics, applied load, sliding speed and sliding distance affect the dry sliding wear and friction of MMCs. However, they conclude that, at higher normal loads (60N), severe wear and silicon carbide particles cracking and seizure of the composites occurs during dry sliding. Liang Y. N. et. al. Reported that the MMCs containing SiC particles exhibit improved wear resistance.
 - **Chandramohan G., et. al[22].** Reported that the sliding distance has the highest effect on the dry sliding wear behavior of MMCs than that of the load and sliding speed.
 - **Y. Reda et.al[23]** Vol.9, No.1 Studies on Al6061-SiC and Al7075 - Al₂O₃ Metal Matrix Composites 45 and R. Clark et. al.[24] In their studies on Al7075 reported that, pre-aging at various retrogression temperatures improves the hardness, tensile properties and electrical resistivity.
 - **Surappa et al 1982 [25].** Noted that aluminum reinforced with 5 % alumina possessed an adhesive wear rate comparable to that of Al-11.8Si or Al-Si hypereutectic alloys. Other work published by the same workers⁴ involving Al, Al-11.8Si, Al-16Si alloys and Al reinforced with Al₂O₃p (5%) indicated that increased silicon content reduced the wear rate.
 - **Hoskings et al.1982 [26]**reported a decrease in adhesive wear rate with increasing particle content (at constant particle size) and dimension (at constant volume fraction) for Al 2014 and 2024 alloys reinforced with Al₂O₃ and SiCp (1-142 pm) of various weight fractions (2- 30 %). SiC was shown to be more effective than alumina in resisting wear, when tested in a ball-on-disc rig. These findings were in disagreement with those reported by Surappa.⁵⁴ However, it should be noted that the former work involved only a small reinforcement content (5 %).

ABRASIVE WEAR:

Abrasive wear occurs when a hard rough surface slides across a softer surface.[1] ASTM International (formerly American Society for Testing and Materials) defines it as the loss of material due to hard particles or hard protuberances that are forced against and move along a solid surface. Standard Terminology Relating to Wear 1987 [9].

Abrasive wear is commonly classified according to the type of contact and the contact environment. The type of contact determines the mode of abrasive wear. The two modes of abrasive wear are known as two-body and three-body abrasive wear. Two-body wear occurs when the grits or hard particles remove material from the opposite surface. The common analogy is that of material being removed or displaced by a cutting or plowing operation. Three-body wear occurs when the particles are not constrained, and are free to roll and slide down a surface. The contact environment determines whether the wear is classified as open or closed. An open contact environment occurs when the surfaces are sufficiently displaced to be independent of one another ASM Handbook Committee 2002 [10].

There are a number of factors which influence abrasive wear and hence the manner of material removal. Several different mechanisms have been proposed to describe the manner in which the material is removed. Three commonly identified mechanisms of abrasive wear are:

1. Plowing
2. Cutting
3. Fragmentation

Plowing occurs when material is displaced to the side, away from the wear particles, resulting in the formation of grooves that do not involve direct material removal. The displaced material forms ridges adjacent to grooves, which may be removed by subsequent passage of abrasive particles. Cutting occurs when material is separated from the surface in the form of primary debris, or microchips, with little or no material displaced to the sides of the grooves. This mechanism closely resembles conventional machining. Fragmentation occurs when material is separated from a surface by a cutting process and the indenting abrasive causes localized fracture of the wear material. These cracks then freely propagate locally around the wear groove, resulting in additional material removal by spalling.

Abrasive wear can be measured as loss of mass by the Taber Abrasion Test according to ISO 9352 or ASTM D 1044.

RESULT AND DISCUSSION:

Effect of orientation on wear

- It is observed that as the orientation of the specimen changes from 0° to 60°, the wear mass (Wt. Loss) decreases from 0.798 gm to 0.626 gm when applied load is 5N.
- It is observed that the wear mass follows the same pattern as in graph 6.1. The wear mass decreases from 0.914 gm to 0.737 gm as the orientation changes from 0° to 60° when applied load is 10N.
- Similarly it is observed that wear mass decreases from 0.937 gm to 0.778 gm the orientation of the specimen changes from 0° to 60° when applied loads is 15N.

Effect of load on wear

- It is observed that the wear mass increases from 0.798 gm to 0.937 gm as the applied load on the specimen increases from 5N to 15N when orientation of the specimen is 0°.
- It is observed that the curve follows the same pattern as in graph 6.5. The wear mass increases from 0.750 gm to 0.886 gm as the applied load on the specimen increases from 5N to 15N when orientation of the specimen is 30°.

- It is observed that the wear mass increases from 0.707 gm to 0.853 gm as the applied load on the specimen increases from 5N to 15N when orientation of the specimen is 45o.

It is observed that the wear mass increases from 0.626 gm to 0.778 gm as the applied load on the specimen increases from 5N to 15N when orientation of the specimen is 60o.

CONCLUSION:

The study of this experimental analysis is an overview of research work on abrasive wear of selected material at different load. It will give you full information about the abrasive wear, its important factors, and techniques used to minimize the wear of aluminum alloy. On the basis of experimental work the following conclusion can be drawn:

- Maximum wear occur when the test specimen is held at 0o angle for given applied load.
- Minimum wear occur when the specimen is held at 60o angle for given applied load.
- As the orientation of the specimen changes from 0o to 60o, the wear mass decreases from 0.798 gm to 0.626 gm when applied load is 5N.
- The wear mass decreases from 0.914gm to 0.737gm as the orientation changes from 0o to 60o when applied load is 10N.
- Wear mass decreases from 0.937 gm to 0.778 gm as the orientation of the specimen changes from 0o to 90o when applied loads is 15N.
- Minimum wear occur when load applied on the specimen is 5N for given orientation load.
- Maximum wear occur when applied load is 15N for the given orientation of the specimen.
- When applied load is varied from 5 N to 15N the wear mass increases from 0.798 gm to 0.937 gm for 0o orientation.
- When applied load is varied from 5N to 15N the wear mass increases from 0.750 gm to 0.886 gm when orientation of the specimen is 30o.
- When applied load is varied from 5N to 15N the wear mass increases from 0.707 gm to 0.853 gm when orientation of the specimen is 45o.
- When applied load is varied from 5N to 15N the wear mass increases from 0.626 gm to 0.778 gm when orientation of the specimen is 60o.

REFERENCES:

1. Rabinowicz, E. (1995). *Friction and Wear of Materials*. New York, John Wiley and Sons.
2. Williams, J. A. (2005). "Wear ad wear particles - Some fundamentals." *Tribology International* 38(10): 863-870
3. Bisson, Edmond E. (1968). *Various Modes of Wear and their Controlling Factors*. NASA Technical Memorendum TMX-52426.
4. Chattopadhyay, R. (2001). *Surface Wear - Analysis, Treatment, and Prevention*. OH, USA: ASM-International.
5. Chattopadhyay, R. (2004). *Advanced Thermally Assisted Surface Engineering Processes*. MA, USA: Kluwer Academic Publishers.
6. Jones, M., H., and D. Scott, Eds. (1983). *Industrial Tribology: the practical aspects of friction, lubrication, and wear*. New York, Elsevier Scientific Publishing Company.
7. Glaeser, W. A., Ed. (1993).
8. Stachowiak, G. W., and A. W. Batchelor (2005). *Engineering Tribology*. Burlington, Elsevier Butterworth-Heinemann
9. *Standard Terminology Relating to Wear and Erosion, Annual Book of Standards, Vol 03.02, ASTM, 1987, p 243-250*
10. *ASM Handbook Committee (2002). ASM Handbook. Friction, Lubrication and Wear Technology. U.S.A., ASMInternational. Volume 18.*
11. Sinmazcelik, T. and I. Taskiran (2007). "Erosive wear behaviour of polyphenylenesulphide (PPS) composites." *Materials in engineering* 28(9): 2471-2477.

-
12. Sinmazcelik, T. and I. Taskiran (2005). *Friction and wear mechanism in nano material.*:21(7) 2133-2137
 13. Bayer, Raymond George (2004) *Mechanical wear*, press pp 112
 14. Chang Chongyi Wang Chenggu and Jin Ying 2010. *Numerical method to predict wheel/rail profile evolution due to wear.* *Wear*, volume 269, Issues 3-4, pp 167-173.
 15. Dharma R. Maddala, Arif Mubarok and Rainer J. Hebert 2010. *Sliding wear behavior of Cu50Hf41.5Al8.5 bulk metallic glass.* *Wear*, Vol 269, 3-4, pp 157-163.
 16. N R Prabhu Swamy, C S Ramesh and T Chandershekar (2010) *Bull. Mater. Sci.*, Vol.33, No. 1, February 2010, pp. 49–54. © Indian Academy of Sciences.49 *Effect of heat treatment on strength and abrasive wear behaviour of Al6061–SiCp composites.*

Mhd Flow and Heat Transfer of A Non-Newtonian Law Fluid Past A Stretching Sheet with Heat Generation/Absorption

B. Shashidar Reddy

Department of Sciences and Humanities, Sreenidhi Institute of Science and Technology, Ghatkesar, Hyderabad, Telangana State, INDIA

ABSTRACT

The present study is to investigate the effects of heat source/sink on convection heat transfer of an electrically conducting, non-Newtonian power-law stretched sheet with surface heat flux. The effects of suction/injection at the surface are considered. The governing equations are transformed into non linear ordinary differential equations using similarity transformation. The set of non linear ordinary differential equations are first linearized by using Quasi-linearization technique and then solved numerically by using implicit finite difference scheme. The solution is found to be dependent on various governing parameters. Velocity and Temperature profiles drawn for different controlling parameters reveal the tendency of the solution.

Keywords: *Non-Newtonian power-law fluid, suction/injection, Surface heat flux and Heat Source/sink parameter.*

INTRODUCTION

The study of flow and heat transfer problems due to stretching boundary has many practical applications in technological processes, particularly in polymer processing systems involving drawing of fibers and films or thin sheets, etc. Sometimes the polymer sheet is stretched while it is extruded from a die. Usually the sheet is pulled through the viscous liquid with desired characteristics. The moving sheet may introduce a motion in the neighboring fluid or alternatively, the fluid may have an independent forced convection motion which is parallel to that of the sheet. Sakiadis [1] was the first to investigate the flow due to sheet issuing with constant speed from a slit into a fluid at rest. Schowalter [2] has introduced the concept of the boundary layer in the theory of non-Newtonian power-law fluids.

For the non-Newtonian power-law fluids, the hydrodynamic problem of the MHD boundary layer flow over a continuously moving surface has been by Mahmoud and Mahmoud [3]. Chiam [4] studied the boundary layer flow of a Newtonian fluid over a stretching plate in the presence of a transverse magnetic field. Pop and Na [5] performed an analysis for the MHD flow past a stretching permeable surface. Recently Chien- Hsin Chen [6] has studied the magneto-hydrodynamic flow and heat transfer of an electrically conducting, non-Newtonian power-law fluid past a stretching sheet in the presence of a transverse magnetic field by considering suction/injection.

Kishan and kavitha [7] studied the MHD heat transfer to non-Newtonian power-law fluids over a wedge with heat source/sink in the presence of viscous dissipation. MHD flow and heat transfer of a non-Newtonian power-law fluid past a stretching sheet with suction/injection and viscous dissipation was studied by Kishan and Shashidar [8]. Kishan and Shashidar Reddy [9] has studied the MHD Effects on non- Newtonian power-law fluid past a continuously moving porous flat plat with heat flux and viscous dissipation. Saritha et al [10] studied Quasi-linearization approach to effects of heat source/sink on MHD flow of non-Newtonian power-law fluid past a continuously moving porous flat plate with heat flux and viscous dissipation.

The present work deals with the flow and heat transfer of electrically conducting, non-Newtonian power-law fluids past a continuously stretching sheet under the action of a transverse magnetic field with suction/injection by taking into account the effect of heat source/sink.

2. MATHEMATICAL FORMULATION

To Construct the model, consider a steady two-dimensional flow of an incompressible, electrically conducting fluid obeying the power-law model past a permeable stretching sheet. The origin is located at the slit through which the sheet is drawn through the fluid medium, the x-axis is chosen along the sheet and y-axis is taken normal to it. This continuous sheet is assumed to move with a velocity according to a power-law form, i.e. $U = Cx^p$, and be subject to a surface heat flux. Also, a magnetic field of strength B is applied in the positive y-direction, which produces magnetic effect in the x-direction. Under the foregoing assumptions and invoking the usual boundary layer approximations, the problem is governed by the following equations:

$$\frac{\partial u}{\partial x} + \frac{\partial v}{\partial y} = 0 \quad (1)$$

$$u \frac{\partial u}{\partial x} + v \frac{\partial u}{\partial y} = \frac{K}{\rho} \frac{\partial}{\partial y} \left(\left| \frac{\partial u}{\partial y} \right|^{n-1} \frac{\partial u}{\partial y} \right) - \frac{\sigma B^2 u}{\rho} \quad (2)$$

$$u \frac{\partial T}{\partial x} + v \frac{\partial T}{\partial y} = \alpha \frac{\partial^2 T}{\partial y^2} + \frac{Q}{\rho C_p} (T - T_\infty) \quad (3)$$

Where u and v are the velocity components, T is the temperature, B is the magnetic field strength, K is the consistency coefficient, n is the flow behavior index, ρ is the density, σ is the electrical conductivity and α is the thermal diffusivity, C_p is the specific heat at a constant pressure and Q is the heat generation constant. The appropriate boundary conditions are given by

$$u_w(x) = Cx^p, \quad v = v_w, \quad \frac{\partial T}{\partial y} = -\frac{q_w}{k} \quad \text{at } y = 0, x > 0 \quad (4)$$

$$u \rightarrow 0, \quad T \rightarrow T_\infty \quad \text{as } y \rightarrow \infty \quad (5)$$

where v_w is the surface mass flux and q_w is the surface heat flux. It should be noted that positive p indicates that the surface is accelerated while negative p implies that the surface is decelerated from the slit. Also note that positive v_w is for fluid injection and negative for fluid suction at the sheet surface.

3. METHOD OF SOLUTION

We shall further transform equations (2) & (3) into a set of partial differential equations amenable to a numerical solution. For this purpose we introduce the variables

$$\eta = \left(\frac{C^{2-n}}{K/\rho} \right)^{1/(n+1)} x^{[p(2-n)-1]/(n+1)} y \quad (6)$$

$$\psi = \left(\frac{C^{1-2n}}{K/\rho} \right)^{-1/(n+1)} x^{[p(2n-1)+1]/(n+1)} f \quad (7)$$

$$\theta_{(n+1)} = \frac{(T - T_\infty) \text{Re}_x^I}{q_w x / k} \quad (8)$$

Where the dimensionless stream function f satisfies the continuity equation with $u = \frac{\partial \psi}{\partial y} = u_w f'$ and $v = -\frac{\partial \psi}{\partial x} = -u_w \text{Re}_x^{-1/(n+1)} \left(\frac{p(2n-1)+1}{n+1} f + \frac{p(2-n)-1}{n+1} \eta f' \right)$.

Under the transformations (6), (7) and (8), the differential equations (2) and (3) reduce to

$$\left(f' \right)^{n-1} f'' + \frac{p(2n-1)+1}{n+1} f f' - p(f')^2 - M f' = 0 \quad (9)$$

$$\frac{1}{\text{Pr}} \theta' + \frac{p(2n-1)+1}{n+1} f \theta' + \frac{p(2-n)-1}{n+1} f' \theta + S \theta = 0 \quad (10)$$

Where primes indicate the differentiation with respect to η .

Subject to the boundary conditions

$$\left. \begin{aligned} f'(0) = 1, f(0) = \frac{n+1}{p(2n-1)+1} f_w, \theta'(0) = -1 \\ f'(\infty) = 0, \theta(\infty) = 0 \end{aligned} \right\} \quad (11)$$

Where

$$M = \frac{\sigma B^2 x}{\rho u_w} \text{ is the magnetic parameter,}$$

$$f_w = -\frac{v_w}{u_w} \text{Re}_x^{1/(n+1)} \text{ is the suction/injection parameter,}$$

$$\text{Pr} = \frac{x u_w}{\nu} \text{Re}_x^{-2/(n+1)} \text{ is the Prandtl number and}$$

$$S = \frac{q_w}{U \rho C_p} \text{ is the Heat Source/Sink.}$$

Where $\text{Re}_x = \frac{\rho u_w^{2-n} x^n}{K}$ is the local Reynolds number. Note here that the magnetic field strength B should

be proportional to x to the power $(p-1)/2$ to eliminate the dependence of M on x , i.e. $B(x) = B_0 x^{(p-1)/2}$ where B_0 is a constant.

The wall shear stress is given by

$$\tau_w = \left[K \left| \frac{\partial u}{\partial y} \right|^{n-1} \frac{\partial u}{\partial y} \right]_{y=0} = \rho u_w^2 \text{Re}_x^{-1/(n+1)} \left| f'(0) \right|^{n-1} f'(0)$$

The physical quantities of engineering interest in this problem are the local skin friction coefficient and the local Nusselt number and local Sherwood number, which are defined respectively by

$$C_f = \frac{\tau_w}{\rho u_w^2 / 2} = 2 \operatorname{Re}_x^{-1/2} |f'(0)|^{n-1} f'(0) \quad (12)$$

and

$$Nu_x = \frac{hx}{k} = \frac{\operatorname{Re}_x^{1/2} \theta(0)}{\theta(0)} \quad (13)$$

$$\text{where } h = \frac{q_w}{T_w - T_\infty} = \frac{k \operatorname{Re}_x^{1/2} \theta(0)}{\theta(0)}$$

4. NUMERICAL PROCEDURE:

The system of coupled, non linear ordinary differential equations (9) and (10) with the boundary conditions (11) are solved numerically. The numerical solutions can be obtained in the following steps:

- Linearize Eq (9) using Quasi Linearization method [11].
- Write the difference equations using implicit finite difference scheme.
- Linearize the algebraic equations by Newton's method, and express them in matrix-vector form and
- Solve the linear system by Gauss Seidal Iteration method.

Since the equations governing the flow are nonlinear, iteration procedure is followed. For the sake of brevity, further details of the solution process are not presented here. The numerical computations were carried out C programming. The numerical solutions of f are considered as $(n+1)$ th order iterative solutions and F are the n th order iterative solutions. After each cycle of iteration the convergence check is performed, and the process is terminated when $F - f < 10^{-4}$.

6. RESULTS AND DISCUSSIONS

The parametric study is performed to explore the effects of magnetic field parameter M , power-law fluid index n , velocity sheet exponent p and suction/ injection parameter fw on the velocity distribution. And the effects of Heat source/sink parameter S , velocity sheet exponent p , power-law fluid index n , and the Prandtl number Pr on the temperature distribution were studied.

Velocity profiles f' are shown in figs.1–4 for different parameters n , M , fw and p . It is observed from fig. 1 that the power-law fluid index n increases as f' increases near the wall and the reverse phenomenon is observed away from the wall. Figs. 2 and 3 show that the effect of magnetic field M and suction parameter fw decelerates the fluid motion for both the cases of pseudo plastic and dilatant fluids. It can be noticed from fig. 4 that the velocity distribution f' decreases as velocity exponent p increases for the both the cases of pseudo plastic and dilatant fluids.

Temperature distributions presented for various values of n , p and Pr are shown in figures 5- 7. Figs. 5(a) and 5(b) represent the temperature profiles for various values of the power-law index n , respectively for an accelerated stretching surface ($p = 1$) and for a decelerated stretching surface ($p = -0.3$). It can be observed from the figures that for the accelerated stretching case fluid temperature decreases as the power-law index n increases, whereas an opposite behavior exist for an decelerated stretching surface. Here, it can be seen that the influence of power-law index n on the wall temperature is more significant for an accelerated stretching surface.

The influence of sheet velocity exponent p on the temperature distributions for $n = 0.5$ (pseudo plastic fluid) and $n = 1.5$ (dilatant fluid) are shown in figs. 6(a) and 6(b) respectively. It is clear from the figures that for a pseudo plastic fluid, a considerable increase in the temperature distribution and the surface temperature are caused by increasing the value of p , but reverse to that increase in p reduces the temperature for a dilatant fluid.

Fig. 7 reveals the effect of generalized Prandtl number Pr on the temperature distribution for shear thinning fluid ($n = 0.5$). It is obvious from the figure that an increase in Prandtl number will produce a decrease in the thermal boundary layer thickness, associated with the reduction in the temperature profiles. The effects of suction/injection parameter and Prandtl number on temperature distribution for dilatant fluids are similar to those for the pseudo plastic fluids.

Figs.8 shows the effect of Heat source/sink parameter on the temperature profiles for both pseudo – plastic and dilatants fluids. From the figures it can be noticed that an increase in the heat source strength, the temperature also increases whereas the temperature decreases with the increase in the heat sink strength.

REFERENCES

- Arya, K.S., "Analysis and Simplification of Three-Dimensional Space Vector PWM for Three-Phase Four-Leg Inverters," *IEEE Transactions on Industrial Electronics*, vol. 58, pp. 450-464, Feb 2011.
- [1] Sakiadis, B.C., "Boundary-layer behavior on continuous moving solid surfaces", *AIChEJ*, vol. 7, pp. 26-28, 1961
- [2] Schowalter, W.R., "The application of boundary-layer theory to power-law pseudo plastic fluid: Similar solutions", *AIChEJ*, vol. 6, pp. 24-28, 1960.
- [3] Mahmoud, M.A.A., Mahmoud, M.A.E., "Analytical solutions of hydro magnetic boundary-layer flow of a non-Newtonian power-law fluid past a continuously moving surface", *Acta Mech*, vo. 181, pp. 83-89, 2006.
- [4] Singh, B., Thakur, C., "An exact solution of plane unsteady MHD non-Newtonian fluid flows", *Indian Journal of pure and applied maths*, vol. 33(7), pp. 993-1001, 2002.
- [5] Pop, I., Na, T.Y., "A note on MHD flow over a stretching permeable surface", *Mech. Res. Comm.*, vol. 25, pp. 263-269, 1998.
- [6] Chien-Hsin Chen, "Effects of magnetic field and suction/injection on convection heat transfer on non-Newtonian power-law fluids past a power-law stretched sheet with surface heat flux", *Int J Thermal Sciences*, vol. 47, pp. 954-961, 2008.
- [7] Kishan, N., Kavitha, P., "Quasi-linearization approach to MHD heat transfer to non-Newtonian power-law fluids flowing over a wedge with heat source/sink in the presence of viscous dissipation", *International Journal of mathematics and computer applications Research*, vol. 3 (5), pp. 15-28, 2013.
8. Kishan, N., Shashidar Reddy, B., "MHD flow and heat transfer of a non-Newtonian power-law fluid past a stretching sheet with suction/injection and viscous dissipation", *International Journal of Applied Mathematical Research*, vol. 1(4), pp. 681-705, 2012.
9. Kishan, N., Shashidar Reddy, B., "MHD effects on non-Newtonian power-law fluid past a continuously moving porous flat plate with heat flux and viscous dissipation", *International Journal of Applied Mechanics and Engineering*, vol. 18 (2), pp. 425-445, 2013.
10. Saritha, K., Rajasekhar, M.N., Shashidar Reddy, B., "Quasi-Linearization approach to Effects of Heat Source/sink on MHD flow of non-Newtonian power-law fluid past a continuously moving porous flat plate with heat flux and Viscous dissipation", *International journal of Applied Sciences and Engineering Research*, vol. 4(1), pp. 36-56, 2105.
11. Bellman, R.E., Kalaba, R.E., "Quasi-Linearization and Non-linear boundary value problems", New York, Elsevier, 1965.

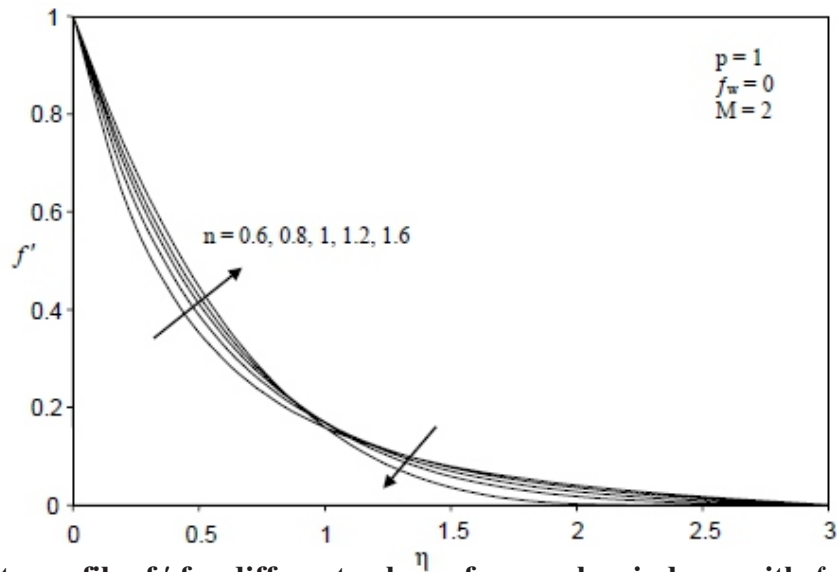


Fig.1. Velocity profiles f' for different values of power-law index n with $f_w = 0$, $p = 1$ and $M = 2$.

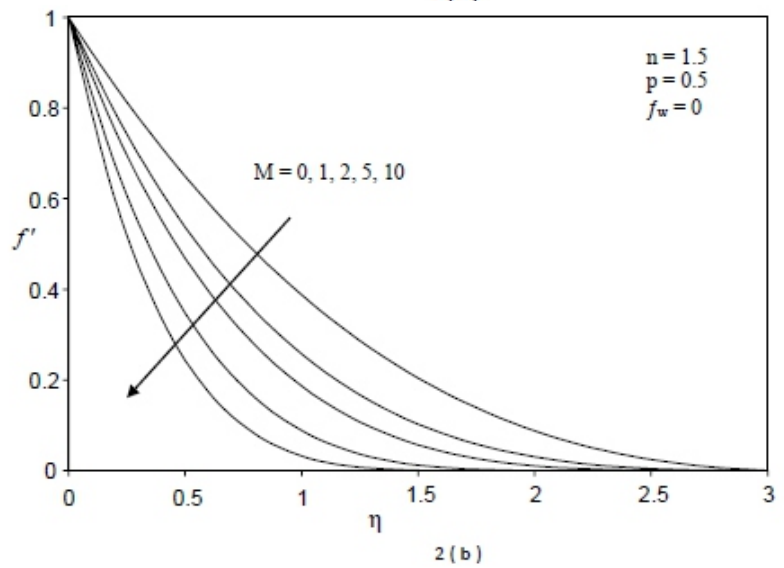
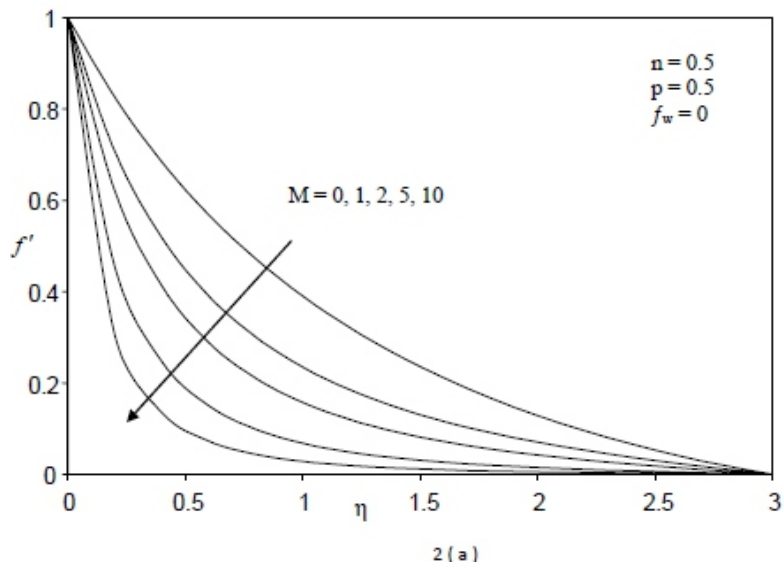


Fig.2. Velocity profiles f' for different values of Magnetic parameter M with $p = 0.5$ and $f_w = 0$. (a) $n = 0.5$; (b) $n = 1.5$

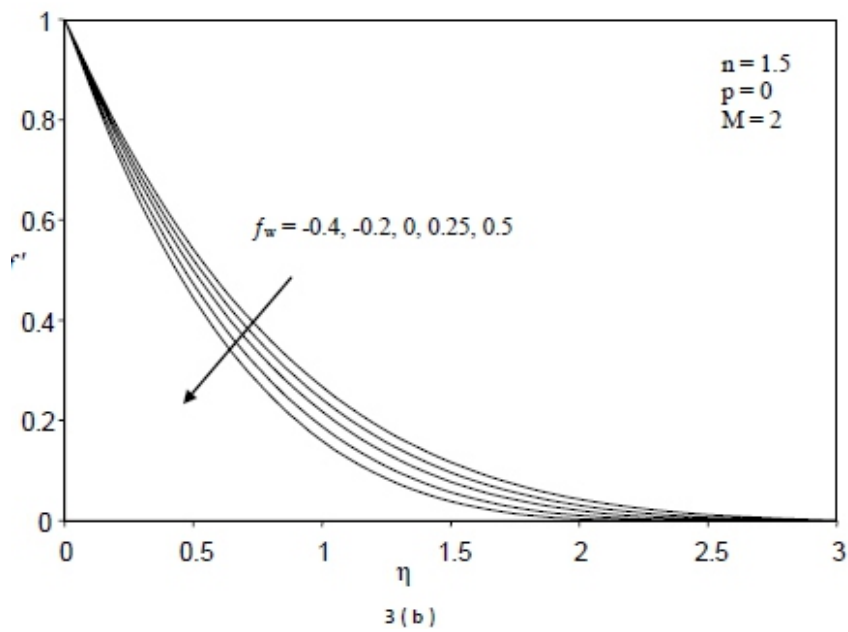
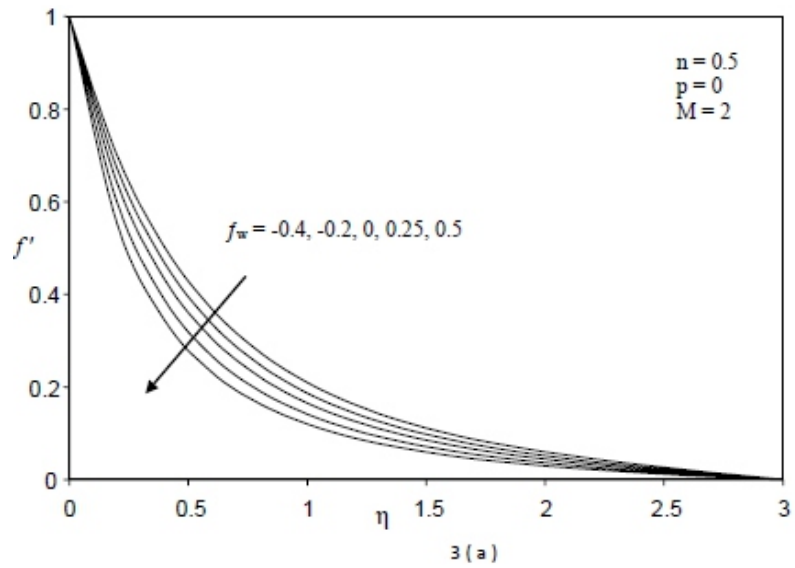
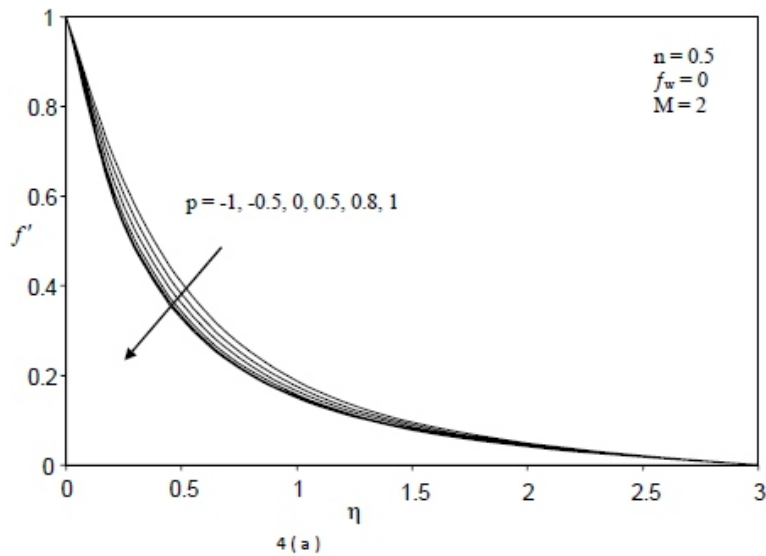


Fig.3. Velocity profiles f' for different values of suction/injection parameter f_w with $p = 0$ and $M = 2$. (a) $n = 0.5$; (b) $n = 1.5$



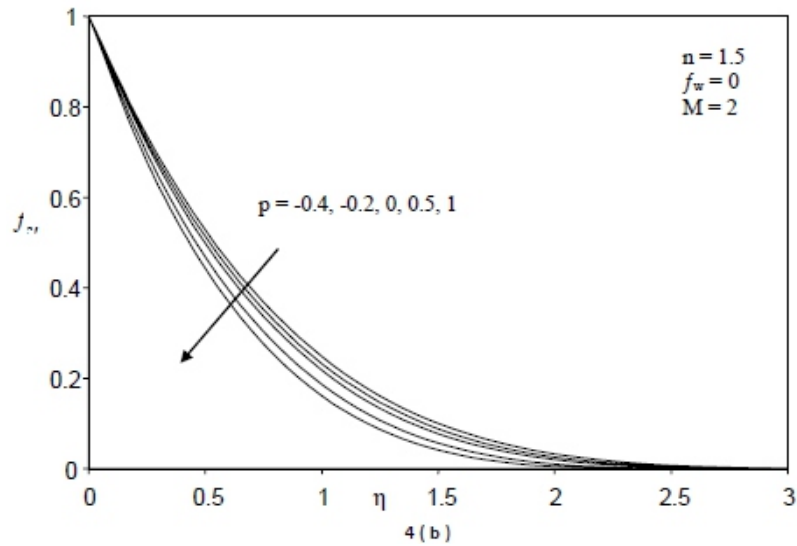


Fig.4. Velocity profiles f'' for different values of sheet velocity exponent p with $f_w = 0$ and $M = 2$. (a) $n = 0.5$; (b) $n = 1.5$

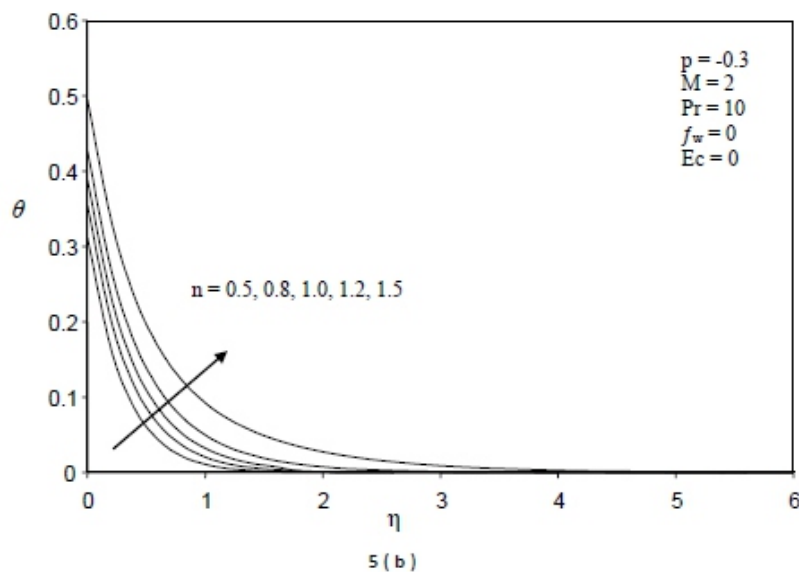
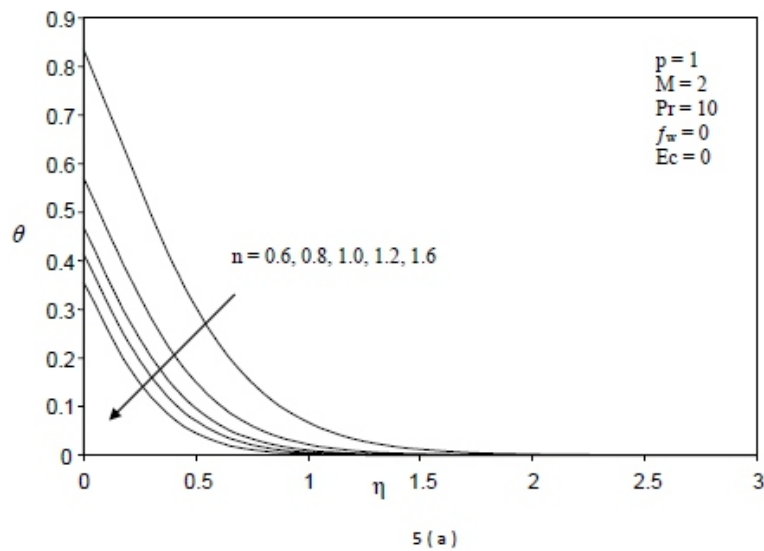


Fig.5. Temperature profiles for different values of power-law index n with $M = 2$, $Pr = 10$, $f_w = 0$ and $S=0$. (a) $p = 1.0$; (b) $p = -0.3$

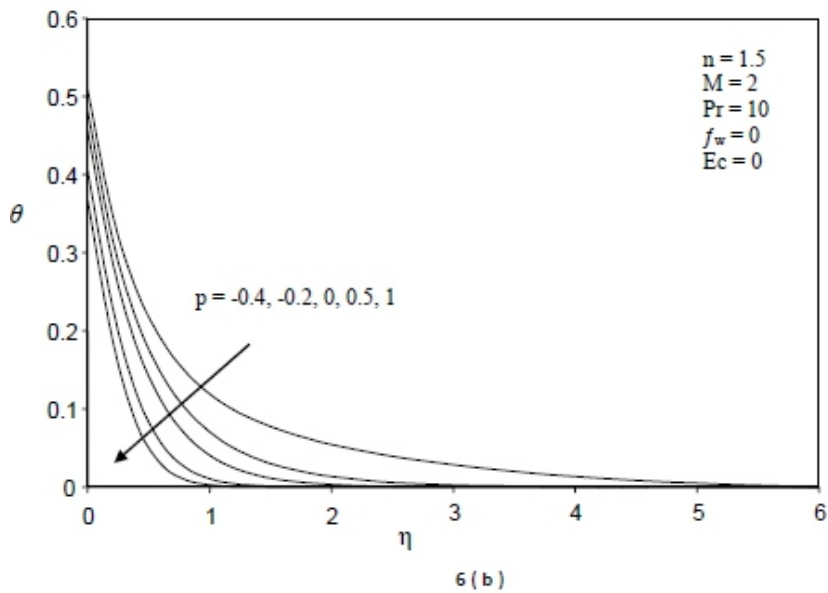
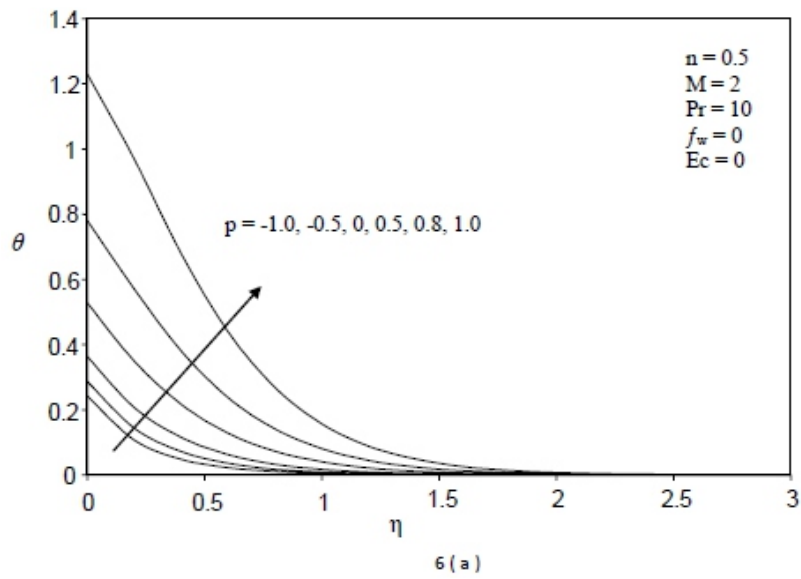


Fig.6. Temperature profiles for different values of sheet velocity exponent p with $M = 2$, $Pr = 10$, $f_w = 0$ and $S = 0$. (a) $n = 0.5$; (b) $n = 1.5$

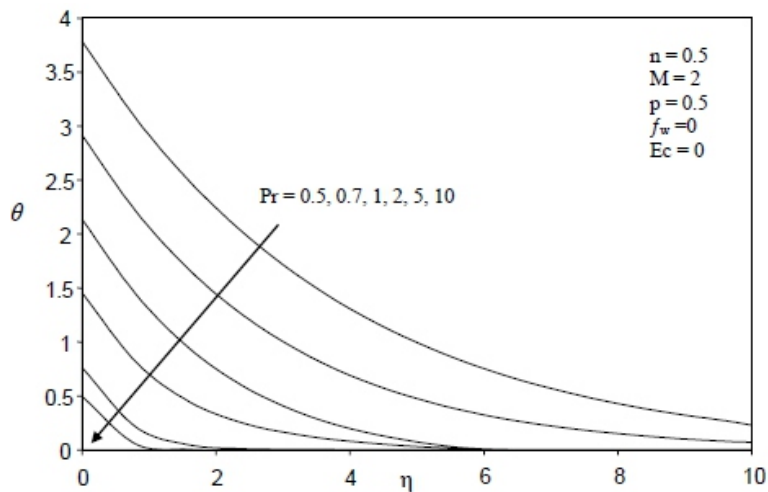
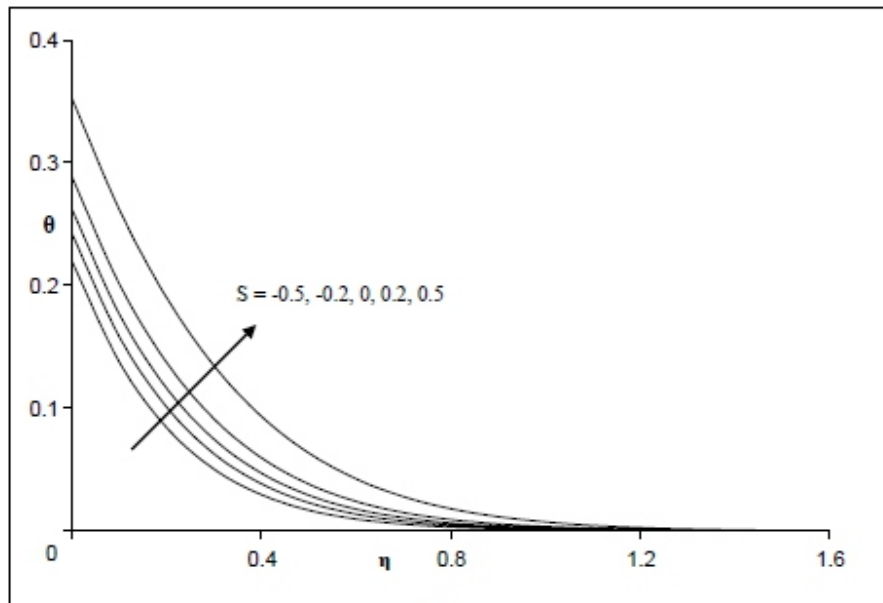
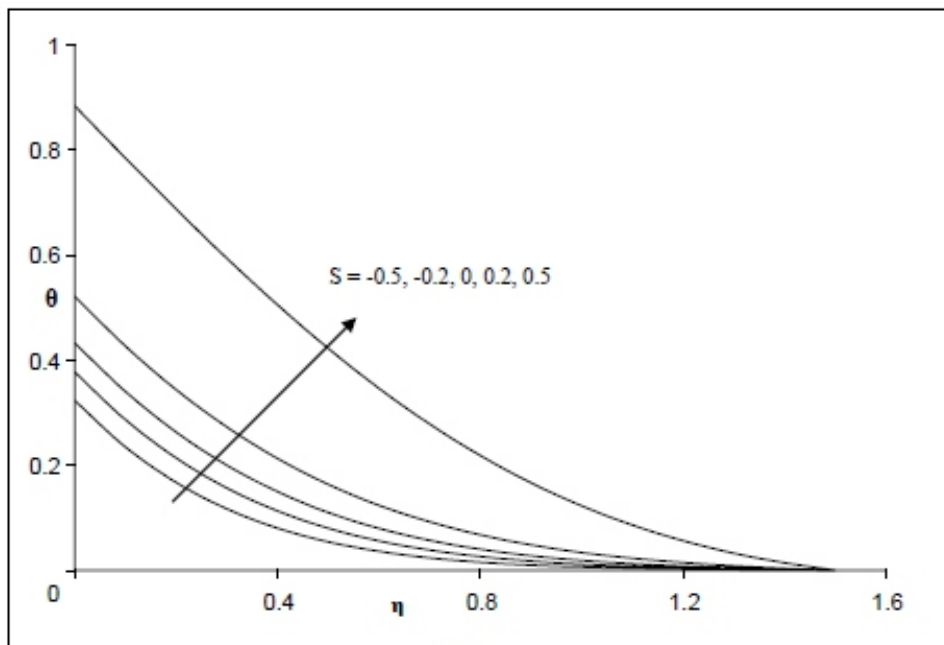


Fig.7. Temperature profiles for different values of Prandtl number Pr with $n = 0.5$, $M = 2$, $p = 0.5$, $f_w = 0$ and $S = 0$.



8 (a)



8 (b)

Figure 8: Temperature profiles for different values of Heat Source/Sink S with $M = 2$, $Pr = 10$, $f_w = 0$. (a) $n = 0.5$; (b) $n = 1.5$

Measurement of Radiation from Naturally Occurring Radioactive Materials in a Mineral Called “Ewoa”, Gurage Zone, Ethiopia.

T. Tessema Teklemariam* W.Tsegaye Birhanu*

*Jimma University, Department of Physics, Nuclear and Radiation Physics Team, Jimma, Ethiopia.

** Gondar University Department of Nuclear and Radiation Physics, Gondar Ethiopia.

ABSTRACT

Using an experimental technique (NaI(Tl)-gamma spectroscopy) the natural radioactivity emanating from a mineral soil which is in use in far-flung areas of Ethiopia was determined. The results of the experiment were converted in to radiation dose units and it is compared with internationally set standards for a public. The calculated average absorbed dose rate in air due to gamma ray from the mineral soil activity, likewise the average hazard indexes obtained for both external and internal exposure do not exceeded the limits set by United Nations Scientific Committee on the Effects of Atomic Radiation (UNSCEAR). Therefore the mineral soil does not pose a threat to the public.

Keywords: Gamma spectroscopy; Naturally Occuring radioactive Materials; Mineral Soil; Radiation dose.

1. INTRODUCTION:

Natural radioactivity is the major contributor to ionizing radiation in environment that comes from both natural background and man-made sources [1]. Most of these radio nuclides are long half-lives which will remain in the environment even after millions of years. Some of these radionuclide and their progenies are emitting gamma rays, which become one of the major sources for external and internal exposure that can cause soft tissue cancers, like lung cancer [2]. Naturally abundant radionuclide (^{226}Ra ; ^{232}Th and ^{40}K) in the environment and releases from fertilizers, agrochemicals, research and medical facilities forms the bulk of radionuclide in ground and surface water, [3]. Therefore presence of radioactivity in contaminated environment can be attributed to naturally occurring and or artificially induced sources. Naturally occurring radioactivity is due to bedrock formations which are weathered, resulting in mineral leaching that leads to contamination [4].

Artificial radioactivity is due to human activities. Contaminations are mainly as a result of agriculture, medicine, research as well as other activities like mining and milling of mineral ore which exposes the earth surface. All this contamination may have health effect [5]; that poses great danger to human and other living organisms. Early investigations in soil and rock (i.e., components of earth's crust) showed that there are measurable amounts of radionuclide such as Uranium and Thorium. Some of radioactive gaseous isotopes are released to the atmosphere. Radium-226 produces Radon-222 via alpha decay which diffuses from the earth into the atmosphere producing a number of short lived radio nuclide; inhalation of the radiation in larger doses can produce lung cancer [2]

In south-western rural region of Ethiopia people are using a mineral soil; locally called “EWOA”, as an additive for cabbage cooking, as a soap to wash cloths and as a mineral additive for livestock. The mineral soil can not be found by digging the ground everywhere in the region, but only in some areas of the region during winter, for this reason the people living in this region purchases the soil from local

markets in the winter season and store larger amount of the soil inside their home to be used in the other seasons of the year. Most people in the surrounding commonly are affected by cough; they locally call it “Gheri” to mean cold air. Sometimes domestic animals are seen to be affected by cough. In this research we want to experimentally determine the amount and the hazardous level of naturally occurring radiation in the mineral soil EWOA in order to check if the cough, Gheri, which is common in animals and people in the surrounding has some connection with the radioactive dose emanating from the soil.

2. RESEARCH METHOD:

To determine the radiation emanating from the mineral soil due to NORM, an experimental technique NaI(Tl) gamma spectroscopy was used. Materials: During the experiment the following devices and chemicals were used. NaI(Tl) gamma spectroscopy, (MCA) multi channel Analyzer, High power supply, pre-amplifier, Post amplifier, Signal Acquisition software (MAESTRO), Desktop computer, IAEA-RGKUTh energy and efficiency calibration standard, quality assuring standards (IAEA-RGU-1, IAEA RGK-1 and IAEA-RGTh-1), four sample holders which exactly fit the space left for a sample inside NaI(Tl) detector container, wax, plastic sheet, masking tape and data log sheet. Method: The major technique employed in to the analysis of the samples for concentration Naturally Occurring Radioactive Materials the Gamma Spectroscopy using NaI(Tl) detector because the resolution of the detector is not very important as the spectrum contains well separated peaks. Three samples of the mineral soil were collected from three known mining areas in the region (“Agena, Shamene, and Bojebbar”). The samples were kept opened to dry at ambient temperature at laboratory in a clean environment, which were later carefully packed into polyethylene bags and transported to the Center for Energy Research and Training, Zaria, Nigeria for further preparation, Gamma spectroscopy count and analysis in accordance with IAEA method.

Experiment: The three soil samples were dried at ambient temperature, powdered and packed fully inside three different sample holders, of height 7cm by diameter 6cm to fit with the sample putting space left inside the lead shielding of the NaI(Tl) detector, as shown in the fig.1 below. The samples were weighed 300g each. The three samples were carefully sealed to prevent radon escape using wax, plastic sheet and masking tape. The sealed samples were (coded as SS001 for Agena mining, SS003 for Shamene mining, and SS005 for Bojebbar Mining) kept for more than twenty days before the counting was started in order to attain secular equilibrium between ISSN: 2320-0294 & Impact Factor: 6.765 progenies and the parent. Before the gamma spectroscopy is used to detect gamma radiation from the samples, energy and efficiency calibration of the detector was performed using a calibrator standard, IAEA-RGKUTh which was sealed inside a container equivalent to sample holders.

After having the energy and efficiency calibration data, IAEA NORM standards (IAEA-RGK-1, IAEA-RGU-1 and IAEA-RGTh-1) containing known amount of the radioactive elements were counted for the purpose of quality assurance or checking the correctness of the measurement system. Analyzing the standards' activity counted with the present setup and compared with the known values given in the certificates of the standards [6]. This helps to check the system is working effectively. Having checked the counting system is correct in the 95% level of confidence, the three samples were counted one by one for 29,000 seconds each with exactly the same condition of counting of the standards. In order to get lab background concentration an empty sample holder was put in to the sample space and counted for twelve hours in a similar procedure as the samples.



Figure 1. Sealed samples of the mineral soil inside a sample holder.

3. RESULTS AND ANALYSIS.

From the experimental data; Geometry dependent peak efficiency of the detector, the concentration of radioactive materials in the standards, the concentration of radioactive materials in the soil samples, counting laboratory background concentration of radioactive materials, doses of radiation due to the soil, internal and external hazard effects due to the radiations, were analyzed. The analyzed data were given in tables. Energy calibration: The graph shown in fig 2 shows the energy calibration for the NaI(Tl) gamma spectroscopy during the measurement. Using the linear fit equation of the curve it was easy to find the channel at which the energy peaks were arrived.

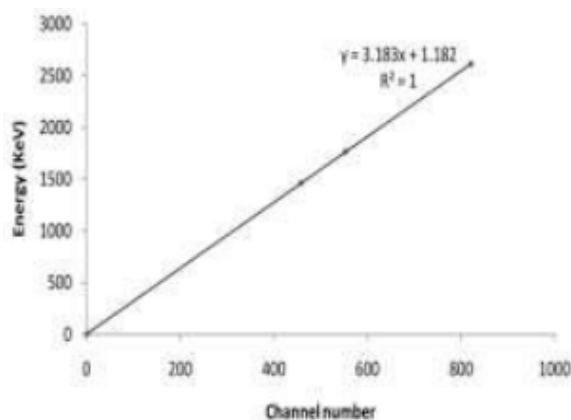


Figure 2. Energy calibration curve of NaI(Tl) gamma detector using the energy calibration mixed standard IAEA-RGKUTh.

Efficiency calibration: The peak efficiencies of the detector for the three peaks were determined using a mixed standard calibrator at the same geometry as the geometry used for the counting of the samples. The value of the efficiencies for each peak was used in the calculation of activity concentrations of NORM in the samples.

Lab Background: The measured activity from the lab background at a specified energies, counted for 12Hrs have been subtracted from the activity of the soil samples. The spectrum obtained during the counting of lab background was as shown in the fig 3. Since NORM occurs everywhere on the crust, the

spectrum shows the expected activities from the norm of the background materials in the room, (roof, wall, ceiling, etc.) but with small concentration.

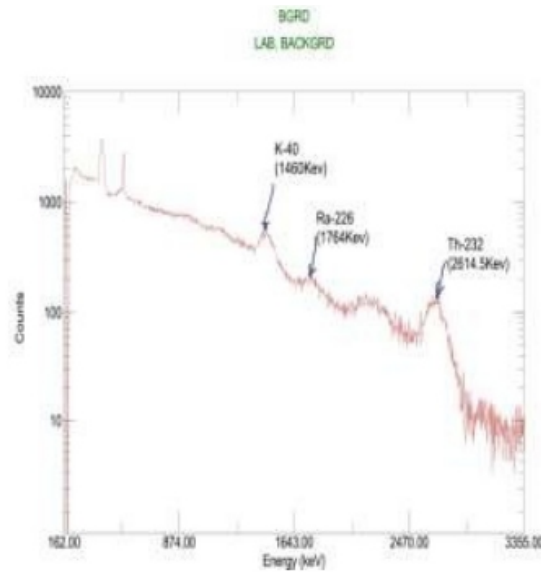


Figure 3: Activity spectrum from NORM in the room background.

Concentration of radioactive materials in the reference: For the purpose of checking the quality of the experimental detection of activities by the experimental set up and analysis in this work, three IAEA standards were measured and analyzed before the measurement of the mineral samples. The spectrums of the counting of the reference materials using the experimental set uop were as shown in the figures Fig. 4, Fig 5 and Fig.6.

The results obtained by the analysis of the reference materials were compared with the values in the certificates which are given with 95% confidence of interval (95%C.I) [6], as shown in the table 1.

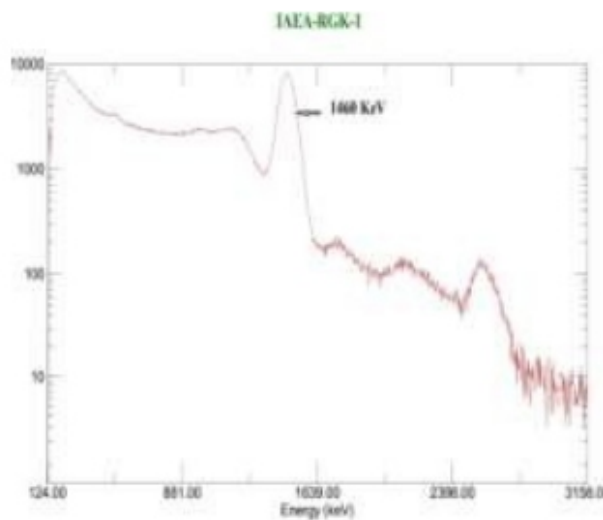


Figure 4: The spectrum obtained by the IAEA standard (IAEA/RGK-1) showing the potassium energy peak.

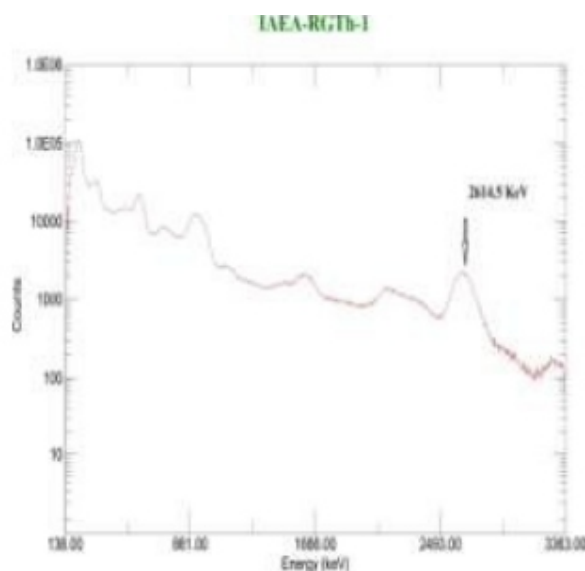


Figure 5: The spectrum obtained by the IAEA standard (IAEA-RGTh-1), showing the gamma peak of Thorium-232.

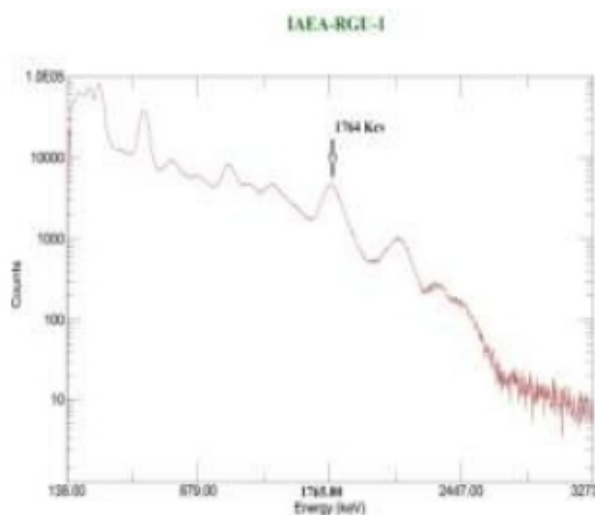


Figure 6: Spectrum of the Uranium standard IAEA-RGU-1, showing the energy peak of Radium-226.

Analyte	IAEA	Concentration (Bq/Kg)	
	Stand	Certificate 95% C.I.	This work
40K	RGK-1	13600 to 14400	13950 ±30.48
226Ra	RGU-1	4910 to 4970	4942±4.90
232Th	RGTh-1	3160 to 3340	3279±28.20

Table 1: Activity concentration of radioactive nuclides in IAEA reference materials obtained during the experimental work compared with the values in the certificate.

As could be seen from Table 1 the experimental set up was acceptable because the results of analysis of the concentration of NORM in the reference materials were in a good agreement with the certified values in the certificates with 95% interval of confidence. Thus the same procedure was carried out on the mineral soil samples with the same geometry of detector to sample position and set up.

Concentration of radioactive materials in the soil samples: Three samples of the mineral soil each were taken from three different mining places were coded SS01, SS03 and SS05, as shown in fig. 1, had been measured. The spectra that were generated from samples during spectrometric analysis, one of such spectrum was shown in the Fig. 8, was used in identification of the radionuclide and analysis of the concentration of each radionuclide in the samples. The result of the analysis was shown in the Table 2. The concentration after the laboratory background is subtracted from the activity of the soils was as shown in Table 2.

Sample ID	C (Bq/Kg)		
	K-40	Ra-226	Th-232
SS01	437.01±3.11	24.33±0.46	72.90±0.11
SS03	438.57±2.80	22.02±0.35	31.93±0.11
SS05	433.90±3.26	27.80±0.46	76.39±0.23

Table 2: Concentration in (Bq/kg) of ⁴⁰K, ²²⁶Ra, and ²³²Th for the mineral soils collected at three mining locations.

The activity (C) is reported in Bq/kg (Becquerel per kilogram) on the basis of the soils dry weight, calculated using the conversion factors as was used in different literatures [7, 5].

As can be seen from table 2, the concentration of K-40 activity ranges from 433.9±3.26 to 438.57±2.8 in Bq/kg in the mineral soil samples collected from different mining areas. This shows that there is no significant difference between the K-40 activity concentrations of the three mineral soil samples. These obtained activity concentration of 40K is slightly higher when compared to the world average values for sediments, 420 Bq/kg, [2]. But there is a slight difference between the radium concentrations in the three soil samples which lies between 22.02±0.35 and 27.80±0.46 in Bq/kg. If we compare the concentration of radium in the soil samples with the world average concentration values of radium in sediments (32Bq/kg) [2], the mineral soil samples contain less concentration of radium. The reported concentrations in Table 2 indicated that there was concentration difference between SS03 and SS05 in the activity concentration of 232Th, i.e. the mineral soil coded with SS05 obtained from “Bojebar” mining site has activity concentration higher than the activity concentration of 232Th in the soil coded SS03 obtained in the “Shamene” mining site by a factor of about 2.4. The obtained activity concentration of 232Th in Shamene mineral soil is smaller than the world average values for sediments, (45Bq/kg) [6], while the result of the concentration in “Agena” and “Bojebar” mineral soil samples show higher concentrations of 10Th compared to the world average of sediments (45Bq/kg) [6].

Absorbed Dose Rate, Annual Effective dose equivalent, External Hazard and Internal Hazard Indexes of the Soil: The absorbed dose rates due to the emitted gamma rays at 1m above the ground for the activity concentration from 226Ra, 232Th and 40K in the samples of the mineral soil were determined as shown in Table 3.

The reported values of, Table 3, absorbed dose values ranges from 50.34±0.358 nGy/h to 82.29±0.509 nGy/h with a rough average of 70.4 nGy/h.

Quantities with units	SS01	SS03	SS05
Absorbed dose rate (nGy/ h)	78.49±0.42	50.34±0.35	82.29±0.51
Effective dose rate (10 ⁻³ mSv/y)	96±0.52	62±0.44	101±0.62
External Hazard index (Hex) (10 ⁻³ mSv/y)	400±2.31	274±1.95	460±2.81
Internal Hazard index (Hin) (10 ⁻³ mSv/y)	466±3.5	317±3.07	496±3.93

* nGy/h = nano gray per hour, *mSv/y = mili severt per year **Table 3: Experimentally determined dose rates and hazard indexes due to Ewoa samples.**

This is within the worldwide value range which is from 18 nGy/h to 93 nGy/h of sediments. The effective annual dose rate due to these radionuclides in the mineral soil was also obtained from Eq.32 and the values ranges from 0.062_0.0004 mSv/y to 0.101_0.0006 mSv/y with an average value of 0.082 mSv/y. This is also less than the average annual dose limit set for radiological assessment which is 1 mSv/y [7]. The external (Hex) and internal (Hin) hazard indexes, which represent the risk associated from exposure to a radiation, for the radionuclide in the samples of the mineral soil was found, the results were as presented in the table 3. From the table 3, it had been shown that the minimum value of (Hex) was 0.274±0.00195 mSv/y and the maximum value 0.460±0.0028 mSv/y with over all rough average of 0.378 mSv/y which is far less than the limit for radiological exposure protection to the public (1 mSv/y) set by International Commission on Radiological Protection [1]. The analysis of the samples SS01, SS03, and SS05 for their internal hazard index (Hin) gives the minimum value 0.317±0.003 mSv/y from the analysis of the sample SS03 and a Maximum value of 0.496±0.0039 mSv/y from the analysis of SS05. The sample SS01 analysis resulted in a value of 0.466±0.0035 mSv/y which lies between the two mineral soil samples and less than the limiting value of radiological exposure protection 1 mSv/y. If the overall average value of the indexes (Hex) and (Hin) of the mineral samples were considered, (0:378 ±0:00236 mSv/y and 0:426±0:0035 mSv/y respectively), they have a value less than 1 mSv/y. This indicated that the risk associated with the mineral soil samples is quite below the limit for radiological exposure protection to the public [1, 8]. The activity concentration value obtained for the mineral soils in this study were found to be within the acceptable limits. Most of the activities obtained were lower than the worlds average values. The calculated effective absorbed dose rate, the average hazard indexes obtained for both external and internal exposure do not exceeded the limits set by ICRP, UNSCEAR [1, 8]

4. CONCLUSION

Based on the analysis of the results, the mineral soil does not pose much threat to the public since the average hazard indexes obtained for both external and internal exposure do not exceeded the limits set by ICRP, UNSCEAR. However, the calculated values were based on exposure at one meter distance from the soil. But in our case, animals and human swallow the mineral soil mixed with food as a spice so that the radiation damage that may be caused may be more intense. Recent studies show that exposure to Ionizing radiation can cause cancer. Washington, DC July 30, 2005 The National Academies of Science released an over 700-page report on the “Health Risks from Exposure to Low Levels of Ionizing Radiation”. The report confirmed that there is no safe level of exposure to radiation that even very low doses can cause cancer [9]. Even exposure to background radiation can cause some cancers.

Low dose of radiation causes other health effects such as heart disease and stroke as reported in [10], and further study is needed to predict the doses that result in these non-cancer health effects.

In this regard the mineral soil since it is taken by animals and human together with food, the existing (the measured amount of radiation dose) in the mineral soil might cause radiation effects. Therefore care should be taken at least in the frequency and amount of taking the mineral soil together with food since larger doses of the mineral could give higher internal radiation dose.

REFERENCES(12PT)

The main references are international journals and proceedings. All references should be to the most pertinent and up-to-date sources. References are written in APA style of Roman scripts. Please use a consistent format for references – see examples below (9 pt):

- [1] <http://www.euronuclear.org/info/encycloped ia/d/decaybasinnatural.htm>, (Accessed on 7/29/2017).
- [2] R.E.Taylor, *Fifty Years of Radiocarbon Dating*, *American Scientist* 88, 60 (2000).
- [3] Szabo, Z. and O.S. Zapezca. *Source and distribution of natural radioactivity in ground water in the Newark Basin, New Jersey. In Radon in Ground Water*, Lewis Publishers (1998).
- [4] Jibiril, N.N. et al., *Radiation Environmental Biophysics*, 46: 53-59. (2007).
- [5] W. Tsegaye Birhanu, A.K Chaubey, et al.. *Determination of Natural Radioactivity Levels of ²³⁸U, ²³²Th and ⁴⁰K in rocks around Gondar city, North-West Ethiopia. International J.of Engineering, Science and Mathematics (IJESM)*, vol. 5, issue 3, page 45-59, (March, 2015).
- [6] IAEA, *Reference products for reference and Trade.*, IAEA/AL/148: (2009).
- [7] Y.A.Ahmed et al., *Journal of Applied Sciences* 6(8):1692-1697,(2006).
- [8] *United Nations Scientific Committee on the Effects of Atomic Radiation (UN-SCEAR), Sources, effects and risks of ionization radiation, Report to The General Assembly, with Scientific Annexes B: Exposures from Natural Radiation Sources*, (New York:UNSCEAR).(2010)
- [9] <https://www.nirs.org/press/06-30-2005/>
- [10] Bjorn Baselet, et al, *Int J Mol Med*. 2016 Dec;

Heat Generation and Uniform Suction/ Blowing of Micropolar Fluid Flow on Porous Plat with Temperature Dependent Viscosity and Thermal Conductivity

Bhairab Borgohian*

* Department of Mathematics,
Tinsukia College, Tinsukia-786125

ABSTRACT

The heat generation of micropolar fluid flow on porous plat with temperature dependent viscosity and thermal conductivity is investigated. The micropolar model due to Eringen is used to describe the working fluid. The partial differential equations governing the motion, angular momentum and energy are reduced to ordinary differential equations using similarity transformations and then solved numerically using Runge- Kutta shooting technique. The effect of the porosity of the medium and the characteristics of the fluid on both the flow and heat transfer is obtained. The results are presented graphically for velocity distribution, temperature distribution and micropolar distributions for various values of non-dimensional parameters. It is found that the effects of the parameters representing variable property of viscosity and thermal conductivity are significant.

Key words: *stagnation point flow, stretching sheet, heat generation, viscosity, thermal conductivity.*

1. INTRODUCTION

The two dimensional flow of a fluid near a stagnation point is a classical problem in fluid mechanics. It was first examined by Hiemenz [4], who demonstrated that the Navier-Stokes equations governing the flow can be reduced to an ordinary third order differential equation using similarity transformation. Later, the problem of stagnation point flow was extended in numerous ways to include various physical effects. The axisymmetric three-dimensional stagnation point flow was studied by Homman [5]. The results of these studies are of great technical importance; for example, in the prediction of skin-friction, as well as heat/mass transfer near stagnation regions of bodies of high speed flows, and also in the design of thrust bearings and radial diffusers, drag reduction, transpiration cooling, and thermal oil recovery. In either the two or three dimensional case, Navier-Stokes equations governing the flow are reduced to an ordinary differential equation of the third order using a similar transformation. The effect of suction on the Hiemenz flow problem has been considered in the literature. Schlichting and Bussman [9] were the first to give the numerical results. More detailed solutions were later presented by Preston [8]. An approximate solution to the problem of uniform suction is given by Ariel [2]. In hydromagnetics, the problem of Hiemenz flow was chosen by Na [7] to illustrate the solution of a third order boundary value problem. Attia [3] studied the investigation of non- newtonian micropolar fluid flow with uniform suction/blowing and heat generation. Stagnation point flow of a non-newtonian micropolar fluid with zero vertical velocity at the surface or heat generation was studied by Amin et al[1].

The viscosity and thermal conductivity assumed to vary with temperature. The wall and stream temperatures are assumed to be constants. Mathematical formulation of the problem under consideration in presented and similarity transformations are applied to reduce the system of partial

differential equations and their boundary conditions describing this problem, into a boundary value problem of ordinary differential equations. The effects of different parameters such as Prandtl number, viscosity parameter, thermal conductivity parameter and microrotation parameter on flow and heat transfer has been studied numerically. The variation of the velocity, microrotation and temperature distribution has been illustrated.

2. MATHEMATICAL FORMULATION OF THE PROBLEM

Consider the two dimensional stagnation point flow of an incompressible non-Newtonian micropolar fluid impinging perpendicular on a permeable wall and flowing away along the x axis. The plane potential flow that arrives from the y-axis and impinges on a flat wall placed at $y=0$, divides into two streams on the wall, and leaves in both directions. The viscous flow must adhere to the wall, whereas the potential flow slides along it. (u,v) are the velocity components at any point (x,y) for the viscous flow, whereas (U,V) are the velocity components for the potential flow. A uniform suction or blowing is applied at the plate with a transpiration velocity at the boundary of the plate given by v_0 , where v_0 for suction. The velocity distribution in the frictionless flow in the neighborhood of the stagnation point is given by $U(x)$, $V(y)$ where the constant $a(>0)$ is proportional to the free stream velocity far away from the surface.

The two-dimensional equations governing the flow in the boundary layer of a steady, laminar and incompressible micropolar fluid are

The equation of continuity

$$u \frac{\partial u}{\partial x} + v \frac{\partial v}{\partial y} = 0 \quad (2.1)$$

The equation of momentum

$$u \frac{\partial u}{\partial x} + v \frac{\partial u}{\partial y} = \frac{\mu + h}{\rho} \left(\frac{\partial^2 u}{\partial y^2} \right) + \frac{h}{\rho} \frac{\partial N}{\partial y} \quad (2.2)$$

The angular momentum equation

$$u \frac{\partial N}{\partial x} + v \frac{\partial N}{\partial y} = \frac{\gamma}{\rho j} \frac{\partial^2 N}{\partial y^2} - 2N \frac{k}{\rho j} - \frac{\partial u}{\partial y} \frac{k}{\rho j} \quad (2.3)$$

and the energy equation

$$u \frac{\partial T}{\partial x} + v \frac{\partial T}{\partial y} = \frac{k}{\rho c_p} \frac{\partial^2 T}{\partial y^2} + \frac{A}{\rho c_p} (T - T_w) \quad (2.4)$$

where N is the micro rotation whose direction of rotation is in the x-y plane, μ is the viscosity of the fluid, ρ is the density and j , γ and h are the micro-inertia per unit mass, spin gradient viscosity and vortex viscosity respectively, which are assumed to be constant, c_p is the specific heat capacity at constant pressure of the fluid, k is the thermal conductivity of the fluid and A is the heat generation/absorption coefficient. The boundary conditions for the problem are

$$u(x,0) = 0, v(x,0) = -v_0, N(x,0) = -n \frac{\partial T}{\partial y}, T = T_w \quad (2.5)$$

$$y \rightarrow \infty : u_{x,y} \rightarrow U, \quad v_{x,y} \rightarrow 0, \quad N_{x,y} \rightarrow 0, \quad T \rightarrow T_\infty$$

Where n is a constant and $0 < n < 1$. The case $n=1/2$ indicates the vanishing of the anti symmetric part of the stress tensor and denotes weak concentration of microelements which will be considered here.

Considering the similarity transformations

$$\eta = \sqrt{\frac{a}{\nu}} y, \quad u = axf', \quad v = -\sqrt{av}f, \quad N = ax\sqrt{\frac{a}{\nu}}g, \quad g \eta = -\frac{1}{2}f'' \quad (2.6)$$

The fluid viscosity is assumed to be inverse linear function of temperature (Lai and Kulacki [6])

as

$$\frac{1}{\mu} = \frac{1}{\mu_\infty} \left[1 + \alpha (T - T_\infty) \right], \quad \frac{1}{\mu} = a (T - T_r), \quad a = \frac{\alpha}{\mu_\infty} \text{ and } T_r = T_\infty - \frac{1}{\alpha} \quad (2.7)$$

where a and T_r are constants and their values depends on the reference state and the thermal property of the fluid. In general $a > 0$ for liquids and $a < 0$ for gases. T_r is transformed reference temperature related to viscosity parameter. α is constant based on thermal property and μ_∞ is the viscosity at $T = T_\infty$. Similarly, consider the variation of thermal conductivity as,

$$\frac{1}{\lambda} = \frac{1}{\lambda_\infty} \left[1 + \xi (T - T_\infty) \right], \quad \frac{1}{\lambda} = b (T - T_k), \quad b = \frac{\xi}{\lambda_\infty} \text{ and } T_k = T_\infty - \frac{1}{\xi} \quad (2.8)$$

where b and T_k are constants and their values depends on the reference state and thermal property of the fluid. ξ is constant based on thermal property and λ_∞ is the thermal conductivity at $T = T_\infty$.

Using equation (6), it can be easily verified that the continuity equation is satisfied automatically and using equation (6)-(8) in the equations (2)-(4) become,

$$f''' = \frac{V_r - \theta}{V_r + K(V_r - \theta)} f'' - \frac{Kg'(V_r - \theta)}{V_r + K(V_r - \theta)} - \frac{V_r \theta' f''}{(V_r - \theta) V_r + K(V_r - \theta)} - \frac{ff''(V_r - \theta)}{V_r + K(V_r - \theta)} \quad (2.9)$$

$$\left(1 + \frac{1}{\gamma} K \right) g'' = K (2g + f'' + f'g - fg') \quad (2.10)$$

$$\theta'' = \frac{EP_r \theta (T_k - \theta)}{T_k} - \frac{\theta' (T_k - \theta)}{T_k} - \frac{\theta'^2}{(T_k - \theta)} \quad (2.11)$$

where $E = \frac{Q}{\rho c_p}$ is the heat generation/absorption parameter.

Prime denotes the differentiation with respect to η and the corresponding boundary conditions are

$$f(0) = A, \quad f'(0) = 0, \quad g(0) = -\frac{1}{2}f''(0), \quad \theta(\eta) = 1 \quad (2.12)$$

$$f'_{\infty} = 1, \quad g_{\infty} = 0, \quad \theta_{\infty} = 0$$

Where $K = \frac{h}{\mu} > 0$ is the material parameter and primes denote differentiation with respect to η .

3. RESULTS AND DISCUSSION

The equations (2.9)-(2.11) together with the boundary conditions (2.12) are solved for various values of the parameters involved in the equations using algorithms based on the shooting method.

Initially solution was taken for constant values of taking $Pr=0.70, G=0.51, K=2.00, V_r = -10.00, T_k = -10.00$ with the viscosity parameter V_r ranging from -10 to -1 at the certain values of $T_k = -10.00$. Similarly the solutions have been found with varying the thermal conductivity parameter T_k ranging from -10 to -1 at the certain values of $V_r = -10$ keeping other values remaining same. We have considered in some detail the influence of physical parameters on velocity distribution, microrotation distribution and temperature distribution which is shown in figures 1-6. Figures 1, 2 and 3 show the velocity, microrotation and temperature profiles with the variation of viscosity parameter V_r . This indicates that both the velocity and temperature distribution decreases as V_r increases where as microrotation distribution increases. Figures 4 and 6 display the temperature profiles for the various values of T_k . From the figures it is seen that the temperatures distribution decreases for the increasing values of T_k . In case of suction, the effect of material parameter on velocity is more pronounced for higher values. From figure 5 it is seen that temperature decreases as Pr increases and the figure bring out the effect of Pr on the thermal boundary layer thickness.

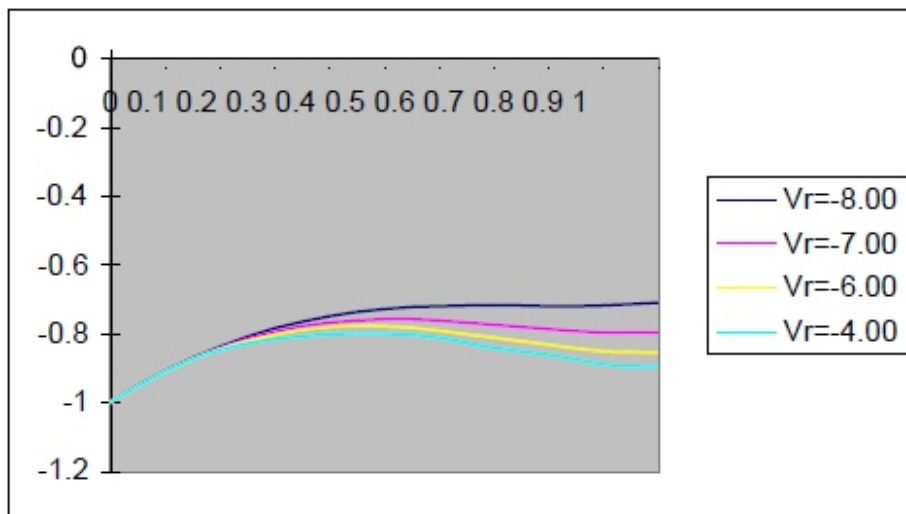


Fig 1: Variation of Velocity profiles for $Pr=0.70, G=0.51, K=2.00, T_k=-10.00$ and different values of V_r .

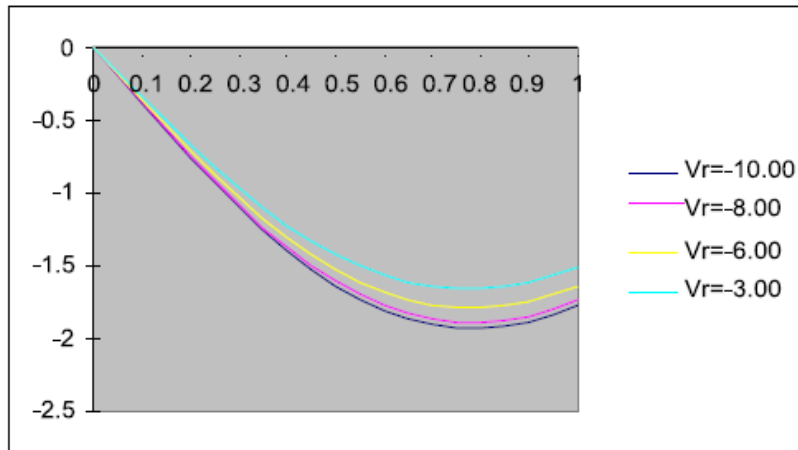


Fig 2: Variation of microrotation profiles for $Pr=0.70$, $G=0.51$, $K=2.00$, $T_k=-10.00$ and different values of V_r .

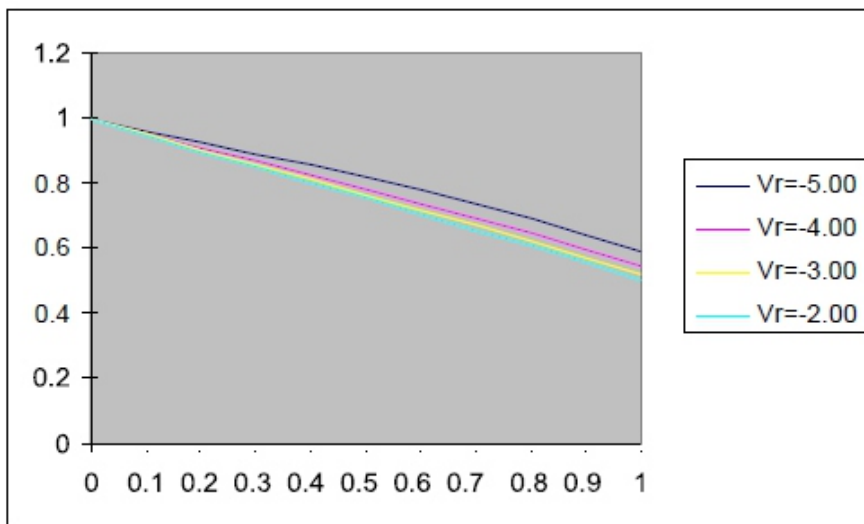


Fig 3 : Variation of temperature profiles for $Pr=0.70$, $G=0.51$, $K=2.00$, $T_k =-10.00$ and for various values of V_r .

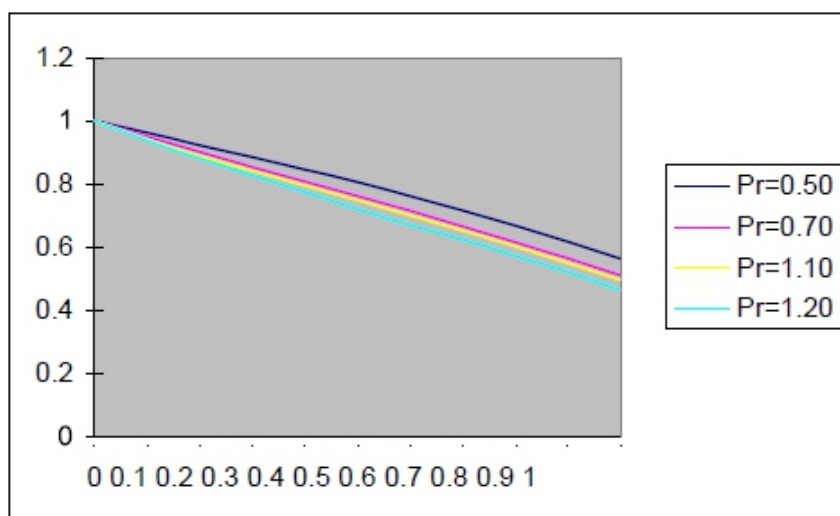


Fig 4 : Variation of temperature profiles for $G=0.51$, $K=2.00$, $V_r=-10.00$, $T_k =-10.00$ and for various values of Pr .

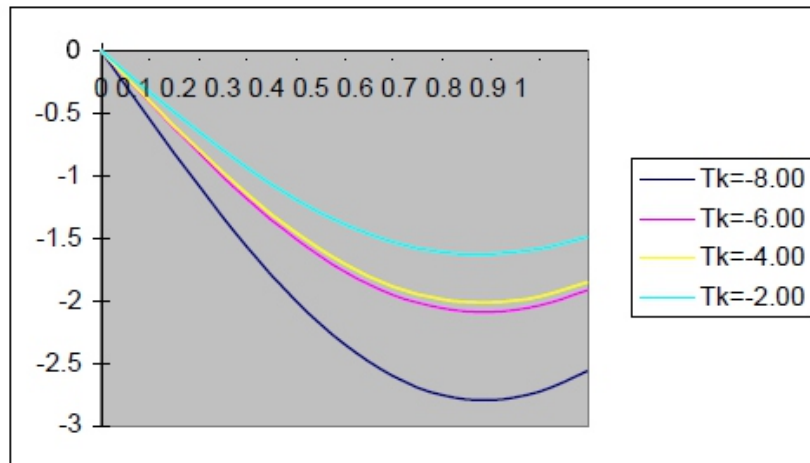


Fig 5: Variation of microrotation profiles for $Pr=0.70$, $G=0.51$, $K=2.00$, $Vr =-10.00$ and for various values of parameter Tk .

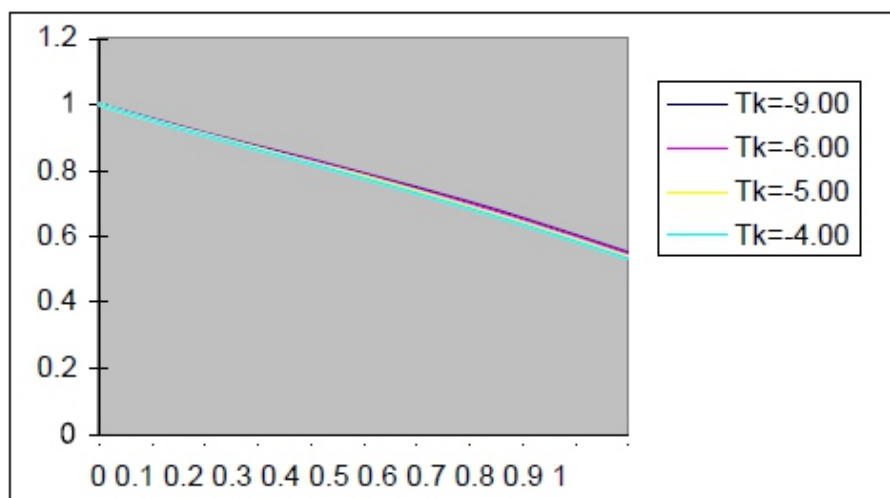


Fig 6: Variation of temperature profiles for $Pr=0.70$, $G=0.51$, $K=2.00$, $Vr =-10.00$ and for various values of parameter Tk .

4. CONCLUSION

In this study the heat generation of micropolar fluid flow on a porous plat with temperature dependent viscosity and thermal conductivity has been investigated.the resulting partial differential equations which describe the problem are transformed into ordinary differential equations by using similarity transformations. Numerical evaluations are performed and graphical results are obtained. The results presented demonstrate clearly that the viscosity and thermal conductivity parameters have a substantial effects on velocity, micropolar and temperature distribution. The effects of Prandtl number is quite significant.

REFERENCES:

- [1] Amin .R. N., Filip. D. and Pop.I., 2004, Stagnation point flow of a micropolar fluid towards a stretching sheet, *Int. J. Non-Linear Mech.* 39 pp 1227-1235.
- [2] Ariel.P.D., 1992, Stagnation point flow with suction: an approximate solution, *J.Appl. Mech.* 61, pp 976-978.
- [3] Attia.H.A., 2006, Investigation of non-Newtonian micropolar fluid flow with uniform suction/blowing and heat generation. *Turkish J.Engineer. Environ. Sci.* 30 pp 359-365.
- [4] Hiemenz. K., 1911, Die Grenzschicht an einem in den gleichformigen flussigkeitsstrom eingetauchten graden Krei-szylinder, *Dingler's Polytech. J.* 326 pp 321-324.

-
-
- [5] Homann.F., 1936, *Der Einfluss Grosser Zahigkeit beider stromung um den Zylinder und um die Kugel*, Z. Angew. Math. Mech. 16, pp153-164.
- [6] Lai F.C. and Kulacki .F.A., 1990, *The effect of variable viscosity on convective heat transfer along a vertical surface in a saturated porous medium*, Int. J. Heat Mass Transfer 33(5) ,pp 1028-1031.
- [7] Na T.Y., 1979, *Computational Methods in Engineering Boundary Value Problem*, Academic Press, New York, pp. 107-121.
- [8] Preston.J.H., 1946, *The boundary layer flow over a permeable surface through which suction is applied*, Reports and Memoirs, British Aerospace research council, London, pp 2244.
- [9] Schlichting .H., and Bussmann.K., 1943, *Exakte Losungen fur die Laminare Grenzschicht mit A bsaugung Ausblasen*, Schri. Dtsch. Akad. Luftfahrt-forschung, Ser.B 725-69

Instructions for Authors

Essentials for Publishing in this Journal

- 1 Submitted articles should not have been previously published or be currently under consideration for publication elsewhere.
- 2 Conference papers may only be submitted if the paper has been completely re-written (taken to mean more than 50%) and the author has cleared any necessary permission with the copyright owner if it has been previously copyrighted.
- 3 All our articles are refereed through a double-blind process.
- 4 All authors must declare they have read and agreed to the content of the submitted article and must sign a declaration correspond to the originality of the article.

Submission Process

All articles for this journal must be submitted using our online submissions system. <http://enrichedpub.com/> . Please use the Submit Your Article link in the Author Service area.

Manuscript Guidelines

The instructions to authors about the article preparation for publication in the Manuscripts are submitted online, through the e-Ur (Electronic editing) system, developed by **Enriched Publications Pvt. Ltd.** The article should contain the abstract with keywords, introduction, body, conclusion, references and the summary in English language (without heading and subheading enumeration). The article length should not exceed 16 pages of A4 paper format.

Title

The title should be informative. It is in both Journal's and author's best interest to use terms suitable. For indexing and word search. If there are no such terms in the title, the author is strongly advised to add a subtitle. The title should be given in English as well. The titles precede the abstract and the summary in an appropriate language.

Letterhead Title

The letterhead title is given at a top of each page for easier identification of article copies in an Electronic form in particular. It contains the author's surname and first name initial, article title, journal title and collation (year, volume, and issue, first and last page). The journal and article titles can be given in a shortened form.

Author's Name

Full name(s) of author(s) should be used. It is advisable to give the middle initial. Names are given in their original form.

Contact Details

The postal address or the e-mail address of the author (usually of the first one if there are more Authors) is given in the footnote at the bottom of the first page.

Type of Articles

Classification of articles is a duty of the editorial staff and is of special importance. Referees and the members of the editorial staff, or section editors, can propose a category, but the editor-in-chief has the sole responsibility for their classification. Journal articles are classified as follows:

Scientific articles:

1. Original scientific paper (giving the previously unpublished results of the author's own research based on management methods).
2. Survey paper (giving an original, detailed and critical view of a research problem or an area to which the author has made a contribution visible through his self-citation);
3. Short or preliminary communication (original management paper of full format but of a smaller extent or of a preliminary character);
4. Scientific critique or forum (discussion on a particular scientific topic, based exclusively on management argumentation) and commentaries. Exceptionally, in particular areas, a scientific paper in the Journal can be in a form of a monograph or a critical edition of scientific data (historical, archival, lexicographic, bibliographic, data survey, etc.) which were unknown or hardly accessible for scientific research.

Professional articles:

1. Professional paper (contribution offering experience useful for improvement of professional practice but not necessarily based on scientific methods);
2. Informative contribution (editorial, commentary, etc.);
3. Review (of a book, software, case study, scientific event, etc.)

Language

The article should be in English. The grammar and style of the article should be of good quality. The systematized text should be without abbreviations (except standard ones). All measurements must be in SI units. The sequence of formulae is denoted in Arabic numerals in parentheses on the right-hand side.

Abstract and Summary

An abstract is a concise informative presentation of the article content for fast and accurate Evaluation of its relevance. It is both in the Editorial Office's and the author's best interest for an abstract to contain terms often used for indexing and article search. The abstract describes the purpose of the study and the methods, outlines the findings and state the conclusions. A 100- to 250-Word abstract should be placed between the title and the keywords with the body text to follow. Besides an abstract are advised to have a summary in English, at the end of the article, after the Reference list. The summary should be structured and long up to 1/10 of the article length (it is more extensive than the abstract).

Keywords

Keywords are terms or phrases showing adequately the article content for indexing and search purposes. They should be allocated heaving in mind widely accepted international sources (index, dictionary or thesaurus), such as the Web of Science keyword list for science in general. The higher their usage frequency is the better. Up to 10 keywords immediately follow the abstract and the summary, in respective languages.

Acknowledgements

The name and the number of the project or programmed within which the article was realized is given in a separate note at the bottom of the first page together with the name of the institution which financially supported the project or programmed.

Tables and Illustrations

All the captions should be in the original language as well as in English, together with the texts in illustrations if possible. Tables are typed in the same style as the text and are denoted by numerals at the top. Photographs and drawings, placed appropriately in the text, should be clear, precise and suitable for reproduction. Drawings should be created in Word or Corel.

Citation in the Text

Citation in the text must be uniform. When citing references in the text, use the reference number set in square brackets from the Reference list at the end of the article.

Footnotes

Footnotes are given at the bottom of the page with the text they refer to. They can contain less relevant details, additional explanations or used sources (e.g. scientific material, manuals). They cannot replace the cited literature.

The article should be accompanied with a cover letter with the information about the author(s): surname, middle initial, first name, and citizen personal number, rank, title, e-mail address, and affiliation address, home address including municipality, phone number in the office and at home (or a mobile phone number). The cover letter should state the type of the article and tell which illustrations are original and which are not.

Address of the Editorial Office:

Enriched Publications Pvt. Ltd.
S-9, IInd FLOOR, MLU POCKET,
MANISH ABHINAV PLAZA-II, ABOVE FEDERAL BANK,
PLOT NO-5, SECTOR -5, DWARKA, NEW DELHI, INDIA-110075,
PHONE: - + (91)-(11)-45525005